

# Measuring $\Omega_0$ from the Entropy Evolution of Clusters

Scott T. Kay<sup>1,2</sup> and Richard G. Bower<sup>1,3</sup>

<sup>1</sup> *Physics Department, University of Durham, Science Laboratories, South Rd, Durham DH1 3LE*

<sup>2</sup> *Scott.Kay@durham.ac.uk*

<sup>3</sup> *R.G.Bower@durham.ac.uk*

2 December 2024

## ABSTRACT

We have extended the entropy-driven model of cluster evolution developed by Bower (1997) in order to be able to study the evolution of galaxy clusters in a range of cosmological scenarios. This approach allows us to explicitly separate the contributions from gravitational collapse and changes in the core entropy of the intracluster gas. In this paper, we apply the model to determine whether a preferred value of the density parameter,  $\Omega_0$ , is selected using the latest available X-ray data. We conclude that measurements of the X-ray evolution of clusters cannot by themselves select a particular cosmological model, with or without the presence of the cosmological constant,  $\Lambda_0 = 1 - \Omega_0$ . An additional constraint on the effective slope of the power spectrum is required to break the inherent degeneracy that exists between this and the background cosmology. We have therefore included a theoretical calculation of the  $\Omega_0$  dependence on the power spectrum based on the cold dark matter paradigm, which also fails to pick out a particular value. An independent measurement of the slope of the power spectrum on rich cluster scales points to  $\Omega_0 < 0.75$  (or  $\Omega_0 < 0.7$  for a flat Universe) to 68% confidence, on average for the individual surveys. Stronger limits are obtained by combining the data from the separate surveys, although the results then become sensitive to systematic differences in the survey strategies. We also compare our results with Eke et al. (1998), who constrain  $\Omega_0$  from the evolution of the temperature function. Making the same assumptions about the  $L_x - T$  relation, our results are consistent with their upper limit, but we fail to place a lower limit on the density parameter. We find that the upper limit placed on  $\Omega_0$  is sensitive to the allowed amount of evolution in the  $L_x - T$  normalisation. The constrained range of values of the entropy evolution parameter,  $\epsilon$ , is insensitive to the values of  $\Omega_0$  considered, although is sensitive to changes in the distribution of the intracluster gas.

**Key words:** galaxies: clusters - cosmology: theory

## 1 INTRODUCTION

Clusters of galaxies are the largest virialized mass concentrations in the present-day Universe. Thus, evolutionary studies offer a unique method for directly determining the rate at which such structures grow in mass. This is influenced by the competing effects of the steepness of the density fluctuation power spectrum, characterised by the effective slope,  $n$ , and the current values of the cosmological parameters,  $\Omega_0$  and  $\Lambda_0$  <sup>\*</sup>. In this paper, we explore the possibility that the value of  $\Omega_0$ , or the combination,  $\Omega_0 + \Lambda_0 = 1$  (which produces a flat geometry), can be robustly determined from an approach based solely on the X-ray evolution of galaxy clusters. In order to be successful however, such an approach

needs to overcome two substantially sized obstacles. Firstly, the correspondence between cluster mass and X-ray luminosity is not direct, and is sensitive to the way in which the gas fills the cluster’s gravitational potential well. Secondly, the degeneracy between the cosmological parameters and the effective slope of the power spectrum on cluster scales,  $n$ , must be broken before a unique value can be selected. The first problem can be tackled by measuring the rate of luminosity evolution and calibrating the efficiency of X-ray emission by some other means of mass estimation, such as the luminosity–temperature correlation (e.g. Mushotzky & Scharf 1997) or gravitational lensing effects (Smail et al. 1997, Bower & Smail 1997). The second problem can be approached in several ways. The most straightforward is to adopt a fluctuation spectrum on the grounds of a physical hypothesis, for example the cold dark matter (CDM) model (e.g. Bardeen et al. 1986). Alternatively, an empirical mea-

<sup>\*</sup>  $\Lambda_0 \equiv \Lambda/3H_0^2$ , with the Hubble constant taking the value  $H_0 = 100 \text{ h km s}^{-1} \text{ Mpc}^{-1}$

surement of the power spectrum could be used, for example using the large-scale distribution of rich clusters from redshift surveys (e.g. Tadros, Efstathiou & Dalton 1997) or by derivation from the shape of the cluster temperature distribution function (e.g. Oukbir & Blanchard 1997). Perhaps the most appealing approach would be to use X-ray observations spanning a wide range in redshift and luminosity to separate out the models purely on the basis of their observed evolution. As we show however, this approach requires a substantial increase in both the solid angle and depth presently covered by X-ray surveys.

Numerous approaches to the determination of  $\Omega_0$  have already been presented in the literature (e.g. see Dekel, Burstein & White 1996, for a recent review), which range from direct arguments based on the peculiar motions of galaxies in the local Universe, through indirect methods using the baryon fraction in clusters of galaxies, to measurements of the acoustic peak in the microwave background spectrum. Each of these approaches have their own strengths and measures a different aspect of our overall cosmological model. A value based on the rate of cluster mass growth is appealing since it measures  $\Omega_0$  on the basis of its large-scale effect over a modest factor of the Universe's expansion. Convergence of all these methods will act as confirmation that our global cosmological picture is valid and that no crucial additional physical processes have been omitted.

Discussion of the implications of cluster evolution is also timely given the growing area of sky that has now been exploited in X-ray surveys. These range in strategy from wide-area projects based on the *ROSAT* all-sky survey (Ebeling et al. 1997, De Grandi et al. 1997), *EMSS* (Henry et al. 1992, Gioia & Luppino 1994), and the *ROSAT* North Ecliptic Pole survey (Gioia et al. in preparation), to smaller solid-angle surveys based on serendipitous sources identified in deep *ROSAT* fields (e.g. Rosati et al. 1998, Castander et al. 1995, Scharf et al. 1997, Collins et al. 1997). Some constraints are also available from very deep survey fields (Hasinger et al. 1998, Bower et al. 1996, McHardy et al. 1998) although the area cover by these fields is currently very small. In addition, reliable temperature data is also becoming available for clusters spanning a range of redshifts and luminosities, via the *ASCA* satellite (e.g. Tsuru et al. 1996, Mushotzky & Scharf 1997, Markevitch 1998). These recent advances have motivated our study, but there is also a clear need to identify the places where future observations, based for example on the forthcoming *AXAF* and *XMM* missions are best targeted. One crucial question is whether more progress is to be made by going to lower flux levels, or more uniform surveys covering a wider area of sky.

Our work is related to that of several others in recent literature, representing a range of possible approaches to the problem of cluster evolution. This paper uses a phenomenological model that separates out the evolution of clusters into factors depending on both the evolution of the mass spectrum and processes resulting in heating and cooling of the intracluster gas. The foundations of the model were discussed extensively in Bower (1997, hereafter Paper I), providing both a physical basis and interpretation. It allows us to minimise additional theoretical input into the calculation by using simple scaling relations to translate the properties of the cluster sample at low redshifts into their equivalents at earlier epochs. The approaches used by Mathiesen & Evrard

(1998) and Blanchard & Bartlett (1998) are related, but use an empirical model for the X-ray luminosity calibration and evolution, combined with the Press-Schechter method (Press & Schechter 1974) for the distribution of cluster masses. The approach of Kitayama & Suto (1997) is more different in that they achieve a match to the luminosity function data through varying the epoch at which the clusters must form. In the case of very low values of  $\Omega_0$ , the distinction between the epoch at which a cluster is observed and that at which it is formed becomes important. We have therefore developed the model from Paper I to incorporate this effect. Finally, a method of direct deconvolution has been outlined by Eke et al. (1998) using recent *ASCA* temperature data (Henry 1998). A wide variety of approaches to this topic is clearly desirable in order to indicate the robustness of the underlying principles. We have therefore included in our discussion a comparison between our work and others and we outline the areas of uncertainty that can be considerably improved from further observations.

The layout of this paper is as follows : in §2, we outline the model on which this paper is based and show how it can be readily extended to incorporate evolution in both open ( $\Omega_0 < 1$ ,  $\Lambda_0 = 0$ ) and flat ( $\Omega_0 < 1$ ,  $\Omega_0 + \Lambda_0 = 1$ ), sub-critical density universes. We have also included in this section, our approach to incorporate the effects of the cluster formation epoch. §3 summarises the constraints on the model parameters using currently available X-ray cluster data for a range of cosmologies and we investigate the limits that can, at present, be set by this approach. We also focus on the inherent degeneracy that exists between  $\Omega_0$  and  $n$ , and investigate whether we can empirically distinguish between different cosmological models, using the methods mentioned earlier. The possibility of measuring evolution of the cluster core radius to place further constraints on the model is also discussed. In §4 we summarise our results and investigate the robustness of assumptions made in this model. We also compare the results obtained from this particular approach with the values that have been obtained by other authors, and explore the differences between the proposed models, leading us to consider the overall accuracy of the method. With this in mind, we identify key strategies for future X-ray surveys. Finally, in section §5 we reiterate our conclusions.

## 2 MODELLING THE X-RAY EVOLUTION IN DIFFERENT COSMOLOGICAL SCENARIOS

### 2.1 X-ray Emission and the Cluster Core

It is now well established that X-ray emission from the intracluster medium is dominated by the thermal Bremsstrahlung process, implying that the emissivity scales as  $\rho^2 T^\alpha$ . We use  $\alpha = 0.4 [\pm 0.1]$  for bolometric/wide-band detectors and  $\alpha = 0 [\pm 0.1]$  for low energy bandpasses, although we find that the results are not affected when making changes to these values within the limits quoted in square brackets. Detections of galaxy clusters in this region of the electromagnetic spectrum are thus extremely sensitive to the way in which the intracluster gas is distributed. Surface brightness distributions are generally fitted using the following (so-called  $\beta$  – model) density profile

$$\rho(r) = \rho_c \left[ 1 + \left( \frac{r}{r_c} \right)^2 \right]^{-\frac{3}{2}\beta} \quad (2.1)$$

with  $r_c$  defining the effective core-size and  $\beta$  the rate at which the density falls off with radius. We adopt a constant value of  $\beta = 2/3$  for the main results in this paper (appropriate for a non-singular isothermal distribution, in agreement with the observational average - see Jones & Forman 1984). The emission is thus characterised by a flattening at small scales (typically  $r_c \sim 100 h^{-1}$  kpc), departing from the distribution expected if the gas followed the underlying dark matter, where current  $N$ -body simulations predict  $\rho \sim r^{-1}$  (Navarro, Frenk & White 1997). A plausible physical interpretation was given by Evrard & Henry 1991 (hereafter EH, see also Kaiser 1991), hypothesising that the intracluster gas was pre-heated prior to the cluster's formation and has retained the entropy acquired from this pre-collapse phase. Assuming that any dissipation was negligible, this provides an entropy *floor*,  $s_{\min}^\dagger$ , forcing the gas to build up a mass distribution that reflects this constraint. For an isothermal distribution,  $s_{\min}$  directly corresponds to the core density,  $\rho_c$ . In paper I, this idea was developed further by allowing  $s_{\min}$  to evolve, using the parameterization

$$s_{\min} = s_{\min}(z=0) + c_v \epsilon \ln(1+z) \quad (2.2)$$

where  $\epsilon$  determines the rate of core entropy evolution, which could be dominated by, for example, the gas being shock-heated as a result of merging (implying negative values) or conversely, radiative cooling (positive values). The value  $\epsilon = 0$  corresponds to no net evolution.

We discuss the effects of departure from this paradigm and their implications in section 4.

## 2.2 Evolution in an $\Omega = 1$ Universe

We model the Bremsstrahlung X-ray luminosity using the relation

$$L_x \propto \int_0^{r_{\text{vir}}} r^2 \rho^2 T^\alpha dr \quad (2.3)$$

Using equation 2.1 to describe the density profile, and assuming that the temperature profile of the gas distribution can be described in a similar way, with the characteristic temperature in proportion to the measured emission-weighted temperature of such systems, we can rewrite the integrand in a scale-free manner. With the further assumption that the virial radius,  $r_{\text{vir}}$ , is significantly larger than the cluster core size for the redshifts of interest, the integral can be regarded as a constant, leading to the relation

$$L_x \propto \rho_c^2 r_c^3 T^\alpha \quad (2.4)$$

Using the above definition of specific entropy, it can be shown that the core density evolves as

$$\rho_c \propto T^{\frac{3}{2}} (1+z)^{-\frac{3\epsilon}{2}} \quad (2.5)$$

The above equation clearly illustrates the separate contributions from both the entropy and dynamical evolution of the

system. The core density can be related to the virial density of the cluster by assuming that  $(r_{\text{vir}}/r_c)^2 \gg 1$ , which leads to a simplification of equation 2.1 for evaluation at the virial radius

$$\rho_{\text{vir}} \sim \rho_c \left( \frac{r_{\text{vir}}}{r_c} \right)^{-3\beta} \quad (2.6)$$

Since an  $\Omega = 1$  Universe exhibits self-similar structural evolution in time, any characteristic density must scale with the background value, implying that  $\rho_{\text{vir}} \propto (1+z)^3$ . Coupled with the assumption that  $r_{\text{vir}} \propto (M\rho_{\text{vir}}^{-1})^{\frac{1}{3}}$ , where  $M$  is the virial mass of the cluster, we can obtain a relation for the cluster's core radius

$$r_c \propto M^{\frac{1}{3}} T^{-\frac{1}{2\beta}} (1+z)^{1-\frac{1}{\beta}(1+\frac{\epsilon}{2})} \quad (2.7)$$

The above relations are not appropriate for scaling properties of individual clusters - it is well known that structure hierarchies can take many different forms (Lacey & Cole 1993, Lacey & Cole 1994), even when considering the merger evolution of one particular mass. We use the assumption (known as the Weak Self-Similarity Principle) that these relations are accurate in determining the mean evolution of the population as a whole. This is fully justified if we adopt a scale-free power spectrum of initial fluctuations (Kaiser 1986, Paper I)

$$\Delta^2(k) \propto \delta_+^2(z) k^{n+3} \quad (2.8)$$

where  $\delta_+$  is the linear growth factor (Peebles 1980) and  $n \in [-3, 1]$  for the CDM model. For an  $\Omega = 1$  Universe,  $\delta_+$  is simply proportional to  $(1+z)^{-1}$ . Since linear evolution thus contains no fixed physical scale, the only scale of interest at a given epoch is that which structure becomes non-linear (i.e. as the overdensity,  $\delta$ , approaches unity). This translates to a mass scale by considering the variance of fluctuations in the linear regime inside spheres of comoving radius  $R$

$$\sigma_R^2 \propto \delta_+^2(z) \int_0^\infty \tilde{W}_R^2(k) k^{n+3} d \ln k \quad (2.9)$$

where  $\tilde{W}_R^2(k)$  is the Fourier transform of the top-hat window function. A specific value of  $R$  (and thus  $\sigma_R$ ) will correspond to the scale of objects that are now rich clusters (Evrard 1989, White, Efstathiou & Frenk 1993). This leads to a simple scaling relation for the mass of such objects

$$M \propto (1+z)^{\frac{-6}{n+3}} \quad (2.10)$$

given that  $M = \frac{4}{3}\pi R^3 \bar{\rho}$ . Hence as  $n \rightarrow -3$ , structure formation becomes progressively more rapid.

The gas temperature will correspondingly evolve as

$$T \propto M^{\frac{2}{3}} (1+z) \quad (2.11)$$

assuming that it is proportional to the underlying velocity dispersion of the dark matter. This and the above results therefore allows us to develop a relation for the X-ray luminosity

$$L_x \propto (1+z)^{\frac{3}{2}(\epsilon-1)(2-\frac{1}{\beta})} T^{\alpha+\frac{3}{2}(3-\frac{1}{\beta})} \quad (2.12)$$

The two key observables that we use in this paper are the X-ray luminosity function (XLF) and the luminosity-temperature ( $L_x - T$ ) relation. The first requires the number

<sup>†</sup> we use the definition of specific entropy,  $s \equiv c_v \ln(T\rho^{1-\gamma})$ ;  $\gamma$  is assumed to be 5/3, appropriate for a non-relativistic ideal gas

density evolution of clusters to be modelled, which is generally done using monte-carlo simulations of merger trees within the extended Press-Schechter formalism (Lacey & Cole 1993). However since we are only interested in some characteristic value at any given epoch, we assume that the the number density scales inversely with  $M$ , i.e.  $n(L) \propto (1+z)^{\frac{6}{n+3}}$ , which is a necessary requirement to conserve mass for a self-similar mass distribution. The second is only used in a way that we are allowed to scale the normalisation using the above assumptions. Attempting to constrain the slope of the  $L_x - T$  relation using this approach involves invoking the Strong Self-Similarity Principle which we avoid here (see Paper I for a more detailed discussion).

### 2.3 Extension to $\Omega_0 < 1$ Cosmologies

For a sub-critical density Universe, several major modifications are required to be made to the model. Firstly, we can no longer assume that the dynamical evolution can be written in time-independent form, hence the simple relations for the evolution of the virial quantities will no longer suffice. Even for scale-free fluctuation spectra, additional knowledge is required to relate the typical density of collapsed objects to the background density. For a low density universe, the Weak Self-similarity Principle cannot be rigorously justified since the internal mass structure of the clusters may not be homologous, depending on the epoch at which they collapse. However, these deviations are small in  $N$ -body simulations (e.g. Eke, Navarro & Frenk 1998, for the  $\Omega_0 = 0.3, \Lambda_0 = 0.7$  scenario), and departures from self-similarity can in any case be incorporated into the definition of the  $\epsilon$  parameter. The aim of this paper is to compare the properties of clusters in flat and open universes, and thus our approach is fully adequate.

To relate the dynamical properties of cluster populations to the background properties set by the cosmology, we use the results of the spherical top-hat collapse model (e.g. Lahav et al. 1991). This predicts that that overdense spherically symmetric perturbations depart from the linear regime, turn around and collapse, forming virialised structures with mean internal densities given by the formula  $\rho_{\text{vir}} = \Delta_{\text{vir}} \rho_{\text{crit}}$ , where  $\rho_{\text{crit}}$  is the density required to close the Universe. The quantity  $\Delta_{\text{vir}}$  is a function of the background cosmology and can be approximated by using the following fitting functions (Eke, Navarro & Frenk 1998)

$$\begin{aligned} \Delta_{\text{vir}} &= 178 \Omega^{0.30} (\Lambda_0 = 0) \\ \Delta_{\text{vir}} &= 178 \Omega^{0.45} (\Omega_0 + \Lambda_0 = 1) \end{aligned} \quad (2.13)$$

which returns the familiar value of 178 for  $\Omega = 1$ . Knowledge of  $\Omega_0, \Lambda_0$  and the redshift of collapse,  $z_f$  is sufficient to provide an evaluation.

Secondly, the linear growth factor,  $\delta_+$  evolves more slowly than  $(1+z)^{-1}$  for  $\Omega_0 < 1$  models. The appropriate relations are as follows (Peebles 1980)

$$\begin{aligned} \Omega_0 < 1 : - \\ \delta_+(x) &= 1 + \frac{3}{x} + \frac{3(1+x)^{\frac{1}{2}}}{x^{\frac{3}{2}}} \ln[(1+x)^{\frac{1}{2}} - x^{\frac{1}{2}}] \\ x &= \frac{\Omega_0^{-1} - 1}{1+z} \end{aligned}$$

$$\Omega_0 + \Lambda_0 = 1 : -$$

$$\begin{aligned} \delta_+(y) &= \frac{(y^3 + 2)^{\frac{1}{2}}}{y^{\frac{3}{2}}} \int_0^y \frac{u}{u^3 + 2}^{\frac{3}{2}} du \\ y &= \frac{2(\Omega_0^{-1} - 1)^{\frac{1}{3}}}{1+z} \end{aligned} \quad (2.14)$$

Accounting for these differences produces the following modified scaling relation for the X-ray luminosity

$$L_x \propto T^a (1+z)^b (1+z_f)^c \left[ \frac{\Delta_{\text{vir}}(z_f)}{\Omega(z_f)} \right]^d \quad (2.15)$$

$$a = \alpha + \frac{3}{2} \left( 3 - \frac{1}{\beta} \right)$$

$$b = 3\epsilon \left( \frac{1}{2\beta} - 1 \right)$$

$$c = 3 \left( \frac{1}{\beta} - \frac{3}{2} \right)$$

$$d = \frac{1}{\beta} - \frac{3}{2}$$

The temperature scaling relation becomes

$$T \propto \delta_+(z)^{\frac{4}{n+3}} (1+z_f) \left[ \frac{\Delta_{\text{vir}}(z_f)}{\Omega(z_f)} \right]^{\frac{1}{3}} \quad (2.16)$$

and the number density scales as  $n(L) \propto \delta_+^{-\frac{6}{n+3}}$ .

### 2.4 The Epoch of Cluster Formation

Since the linear growth of fluctuations ‘freezes out’ when  $z \sim \Omega_0^{-1} - 1$  (Peebles 1980), producing the present-day abundance of clusters requires structure to have formed at progressively earlier epochs for lower density Universes. Consequently, the epoch of cluster formation,  $z_f$  can be significantly different from the redshift range of an observed sample, leading to inaccuracies in the scaling properties (Kitayama & Suto 1996). We tackle this problem by defining the epoch of formation to be such that the cluster has acquired a fraction,  $f$  of it’s total mass when observed. Again, taking advantage of the Weak Self-Similarity Principle allows us to scale the characteristic mass at the appropriate time

$$M(z_f(z)) = f M(z) \quad (2.17)$$

Material that has been accumulated between  $z_f$  and  $z$  is assumed to have negligible effects on the normalisation of the mass distribution, even though the total mass and therefore temperature of clusters can change.

The effect that varying  $f$  has on the X-ray luminosity is illustrated in Figure 1 for a typical median redshift of current distant cluster samples ( $z = 0.4$ ). This is done by plotting the following function

$$F(\Omega_0, \Lambda_0, z) = F_0 (1+z_f)^{\frac{11}{4}} \left[ \frac{\Delta_{\text{vir}}(z_f)}{\Omega(z_f)} \right]^{\frac{11}{12}} \quad (2.18)$$

varying with  $\Omega_0$ , i.e. the part of equation 2.15 that depends on  $z_f$ . The constant,  $F_0$  normalises the relation to the corresponding value at the present day ( $z_f(z = 0)$ ). Clearly for the  $\Omega = 1$  case, the formation epoch scales in direct proportion to the observed redshift, with the normalisation only

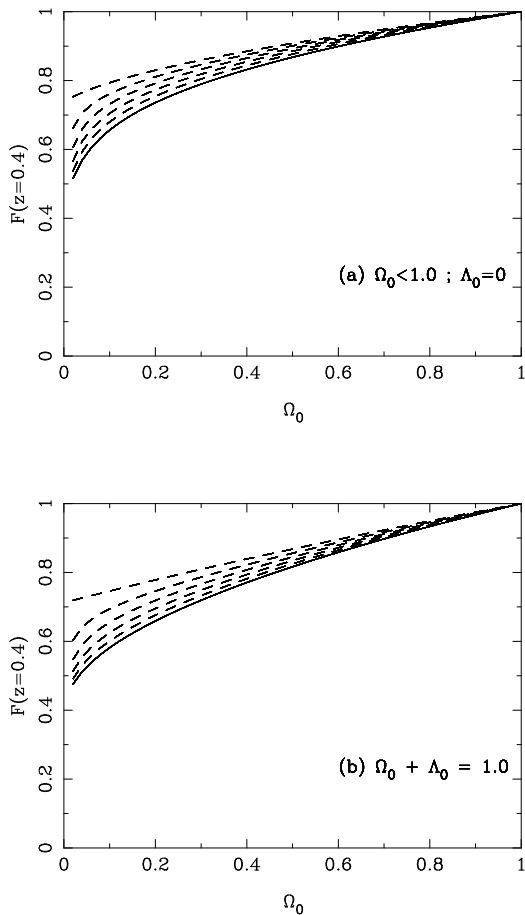


**Figure 1.** The X-ray luminosity factor that depends on the cluster formation redshift,  $z_f$ , as a function of the background cosmology, for both open ( $\Omega_0 < 1$ ) and flat ( $\Omega_0 + \Lambda_0 = 1$ ) models, for the case  $z = 0.4$ . The solid line illustrates the variation of  $F$  for a mass fraction of 1 and the dashed lines show progressively lower values, in steps of 0.1, to  $f = 0.5$ .

depending on the slope of the power spectrum,  $n$  (which also controls the rate at which structure grows). As the matter density drops below the critical value, we see a decrease in about a factor of 2 for  $\Omega_0 = 0.1$ , although the dependence on  $f$  is relatively weak (even for  $\Omega = 0.1$ ): reducing  $f$  from  $1 \rightarrow 0.5$  produces only a 40% change in  $F$ , even in this extreme case. Therefore, we have selected a fiducial value of  $f = 0.5$  for the results that follow.

### 3 USING THE EVOLUTION OF CLUSTERS TO CONSTRAIN $\Omega_0$

Since the essence of the model is to scale characteristic properties of a cluster population from one epoch to another, we need to use data based on local samples in order to normalise the scaling relations detailed in the last section. We can then determine the likelihood distribution of parameters by fitting the scaled relations, controlled by the model parameters, to the data available at higher redshift. At this stage, we have assumed that our free parameters are the slope of the power spectrum,  $n$ , and the entropy evolution parameter,  $\epsilon$ . We have chosen to fix the cosmological density

at four values (with and without the cosmological constant) :  $\Omega_0 = 0.1, 0.3, 0.5, 1.0$ , in order to clearly illustrate the effects of a varying cosmological background on the physical evolution of clusters. Below, we discuss the datasets used to constrain the set  $(n, \epsilon)$  and the corresponding results. All data presented have been compiled with an assumed Hubble constant of  $H_0 = 50 \text{ km s}^{-1} \text{ Mpc}^{-1}$ .

#### 3.1 The Luminosity-Temperature Relation

We place a constraint on the temperature evolution of clusters by making use of the  $L_x - T$  relation, which is at present, adequately described by a fixed power law,  $L_x \propto T^\lambda$ , and fixed intrinsic scatter. We determine the evolution of the  $L_x - T$  relation by fitting a maximum likelihood model to the combined low and high redshift data given by David et al. (1993) and Mushotzky & Scharf (1997), compiled mainly from the *ASCA* and *EMSS* satellites. We assume the distribution of temperatures (that lead to considerable scatter in the relation) are Gaussian distributed, and convert the 90% systematic errors in the temperature measurements (quoted by the authors) to their equivalent  $1\sigma$  values. In order to ensure that there was good overlap in luminosity between the high and low redshift datasets, we limited the comparison to clusters with bolometric luminosities greater than  $10^{44.5} \text{ erg s}^{-1}$ , although the results are not particularly sensitive to this choice. The model for the  $L_x - T$  correlation that we fit includes an adjustable zero-point, slope and intrinsic scatter, as well as a redshift-dependent normalisation term that is parameterized as  $\Delta \log T_0 = \eta \log(1+z)$  (where  $T_0$  is a reference temperature). We determine confidence limits on the evolution of the normalisation by minimising over the other parameters and calculating the distribution of  $C$  values, where

$$C \equiv -2 \sum_{i=1}^N \ln P_i(\eta), \quad (3.1)$$

where the subscript  $i$  runs over each cluster,  $P_i$  is the probability of measuring the cluster with given temperature, luminosity and normalisation, controlled by  $\eta$ . We have assumed that  $\Delta C$  is distributed as  $\chi^2$  with one free parameter (Cash 1979).

This treatment assumes that we are not interested in the slope of the relation. This is exactly true if the luminosities of the clusters do not evolve and the evolution of the  $L_x - T$  relation is due to the temperature evolution of the clusters alone. In practice, however, a particular choice of the parameters  $(n, \epsilon)$  implies correlated changes in luminosity and temperature. For simplicity and consistency with other work, we have converted the evolution in both quantities into a change in temperature at fixed luminosity. This correction involves the slope of the relation, although we emphasise that this is an artefact of the way in which the normalisation is quoted. In principle, each model requires that we examine the likelihood as a function of a combination of  $\eta$  the fitted slope  $\lambda$  (which changes with the choice of  $(n, \epsilon)$  parameters); in practice, however, the slope of the relation is sufficiently constrained that almost identical results (better than 10% accuracy) are obtained if we examine the likelihood as a function of the single parameter  $\eta$  and then simply adopt the best fitting slope in the model calculation.

Parameter	Best Fit	68% (min,max)	95% (min,max)
$\eta$	-0.10	(-0.37,+0.17)	(-0.63,+0.43)
$\lambda$	0.292	(0.310,0.276)	(0.325,0.260)

**Table 1.** Values of the parameters used to fit the (temperature) evolution of the  $L_x - T$  relation, assuming a power law dependence on  $L_x$  with slope,  $\lambda$  and an evolution term between low and high redshift parameterized as  $(1+z)^\eta$ . Shown are the best-fit values of the slope and evolution parameters, as well as 68% and 95% confidence levels on their dispersion, for the median redshift of the high- $z$  sample,  $\langle z \rangle = 0.3$ , and a value of  $q_0 = 0$ .

Survey	$N_{bins}$	$\langle z \rangle$	$N_{clus}$
SHARC (Burke et al. 1997)	4	0.44	16
WARPS (Jones et al. 1998)	4	0.47	11
RDCS (Rosati et al. 1998)	3	0.60	14
<i>EMSS</i> 1 (Henry et al. 1992)	4	0.33	23
<i>EMSS</i> 2 (Luppino & Gioia 1995)	*	0.66	6

**Table 2.** Details of the distant cluster survey XLF's used for constraining evolution of the *ROSAT* BCS XLF. The *EMSS* 2 data is not binned but rather taken as a point in the cumulative luminosity function.

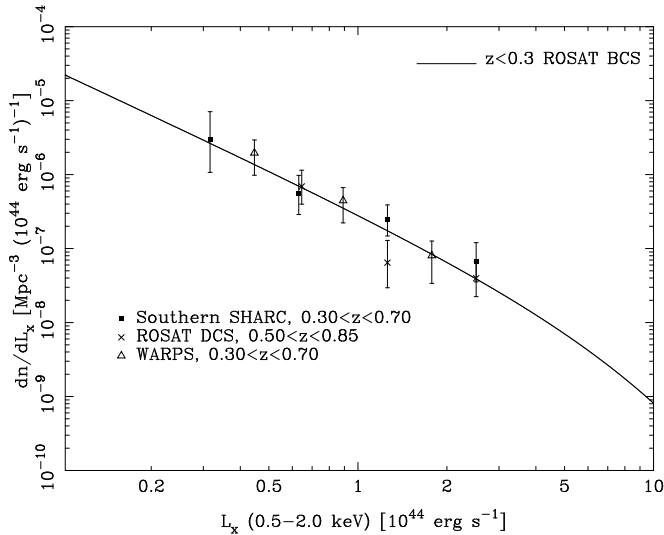


**Figure 2.** The distant cluster X-ray luminosity functions used in this paper, that were compiled from data observed using the *ROSAT* satellite, evaluated in the 0.5 – 2.0 keV pass band. The solid line is the best-fit Schechter function for the *ROSAT* BCS  $z < 0.3$  sample from Ebeling et al. (1997). The square points is the non-parametric XLF from the Southern SHARC survey (Burke et al. 1997), the crosses from the RDCS survey (Rosati et al. 1998) and the triangles from the WARPS survey (Jones et al. 1998). For the purposes of this plot,  $q_0 = 0.5$  ( $\Omega = 1$ ).

The limiting values of the evolution rate parameter are given in Table 1 along with the corresponding slope of the  $L_x - T$  correlation, for the median redshift of the high-redshift sample ( $\langle z \rangle = 0.3$ ) and a value of  $q_0 = 0$  ( $\Omega_0 = \Lambda_0 = 0$ ). These values are converted to the appropriate cosmologies when required, since the normalisation is affected by the assumed value of  $\Omega_0$  through the distance dependence of the luminosity. The uncertainties in the evolution rate are dominated by the intrinsic scatter in the relation. We therefore note that while the evolution of the relation is statistically well defined, it is sensitive to systematic error and selection that may tend to exclude hotter (or colder) clusters.

### 3.2 The X-ray Luminosity Function

The second X-ray observable used in this paper is the cluster X-ray Luminosity function. For simplicity we adopt a Schechter function parameterization

$$\frac{dn}{dL_x} = A \exp\left(-\frac{L_x}{L_x^*}\right) L_x^{-\alpha} \quad (3.2)$$

The local XLF used in this paper is the one given by Ebeling et al. 1997 based on the *ROSAT* Brightest Cluster Sample (BCS), which contains clusters with  $z < 0.3$  selected and flux-limited at X-ray wavelengths. We adopt their best fit parameters to equation 3.2 for the 0.5 – 2.0 keV band, namely [ $A = 33.2 (10^{-8} \text{ Mpc}^{-3} \Delta L^{-1})$ ;  $\alpha = 1.85$ ;  $L_x^* = 5.7 (10^{44} \text{ erg s}^{-1})$ ], shown in Figure 2, and [ $A = 49.5 (10^{-8} \text{ Mpc}^{-3} \Delta L^{-1})$ ;  $\alpha = 1.82$ ;  $L_x^* = 10.7 (10^{44} \text{ erg s}^{-1})$ ], for the 0.3 – 3.5 keV band (shown in Figure 3). Since they find no significant evolution ( $< 1.8\sigma$ ) in their sample, we assume this to represent the XLF at the present day.

In order to place constraints on the observed evolution of the XLF, we have used the distant cluster redshift distributions and luminosity functions that are presently available, summarised in Table 2. Figure 2 illustrates the binned, non-parametric XLF's that have been compiled from *ROSAT* data (SHARC, WARPS and RDCS), with luminosities evaluated in the 0.5 – 2.0 keV band. None of these samples show significant evolution of the cluster XLF, out to typically  $z \sim 0.5$ . Figure 3 shows the *EMSS* 1 XLF in the 0.3 – 3.5 keV band. Clearly, this hints at negative evolution (i.e. a lower space density of clusters of given luminosity at higher redshift), although one must be careful in the sense that evolutionary effects can manifest themselves across the four bins, potentially leading to an overestimation of the evolution if this is not taken into account. We account for this, discussed below. Finally, Figure 4 shows the *EMSS* 2 cumulative point, also in the 0.3 – 3.5 keV band. We assume that it is bright enough not to be incomplete, in the sense that there are no more brighter clusters in the fields studied. Since this point is significantly lower than the BCS XLF, this should provide a tight constraint on  $n$  and  $\epsilon$ .

Ideally, we would constrain our model parameters on the basis of individual clusters using a global maximum likelihood approach. Starting from the present-day luminosity function of Ebeling et al. (1997), we could assign likelihood probabilities to each of the observed clusters (and non-detections) by combining the model X-ray luminosity function at the appropriate redshift with the selection function defined by each of the surveys. This approach would avoid all problems related to redshift binning of the available data, and allow cosmological luminosity distance and angular diameter corrections to be consistently applied.

Unfortunately, the detailed survey selection functions are not generally available to us, so we must adopt an ap-

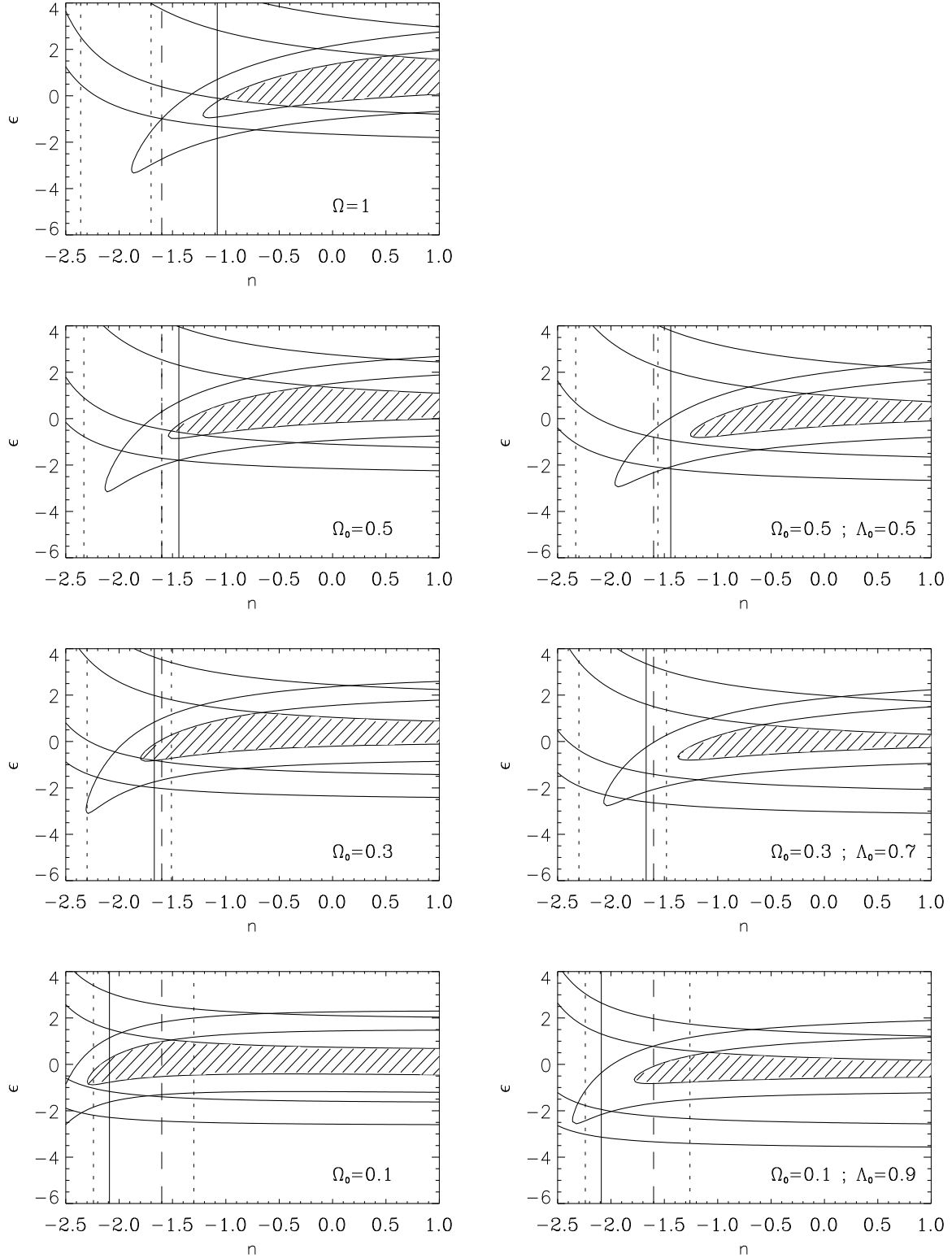


**Figure 5.** Constraints on the slope of the power spectrum,  $n$ , and the entropy evolution parameter,  $\epsilon$  for seven different cosmological scenarios. Top-right to bottom-left contours are the 68% and 95% confidence regions from the evolution of the X-ray luminosity function, using the results of the Southern SHARC survey (Burke et al. 1997). Top-left to bottom-right contours represent the 68% and 95% confidence regions for evolution of the cluster luminosity-temperature relation, making use of data provided by David et al. (1993) and Mushotzky & Scharf (1997). Shaded regions are for parameters consistent with the evolution within 68% limits (of both XLF and  $L_x - T$ ). The vertical solid line is the determination of  $n$  from the CDM based theoretical calculation in Section 3.4, the vertical dashed line is a measured value of  $n$  from the APM rich cluster sample (Tadros, Efstathiou & Dalton 1997) and the vertical dotted lines are the values of  $n$  from the range of  $\Gamma$  as determined by Eke et al. (1998).

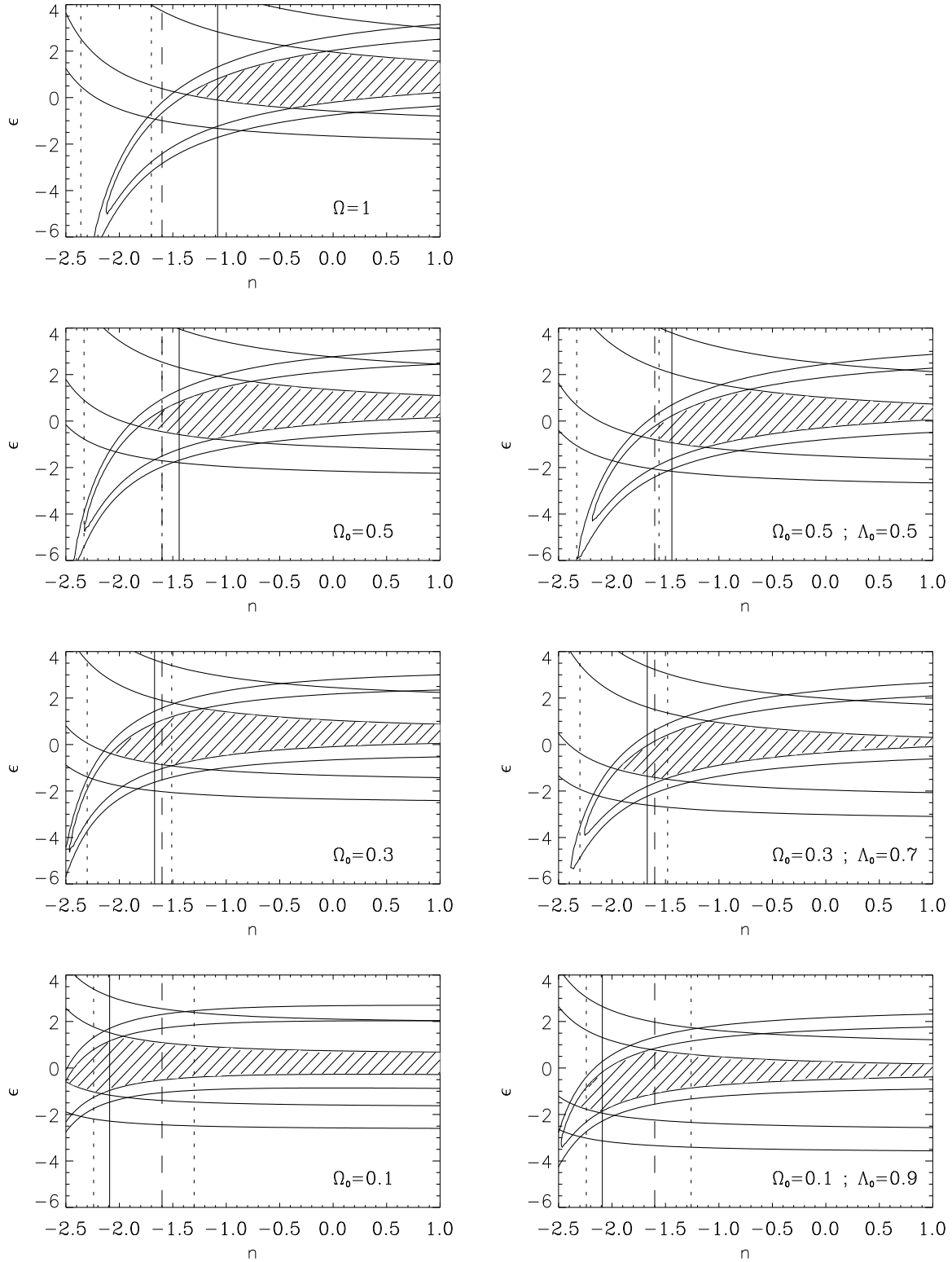


**Figure 6.** Model constraints using the XLF data from the WARPS survey, given by Jones et al. (1998).



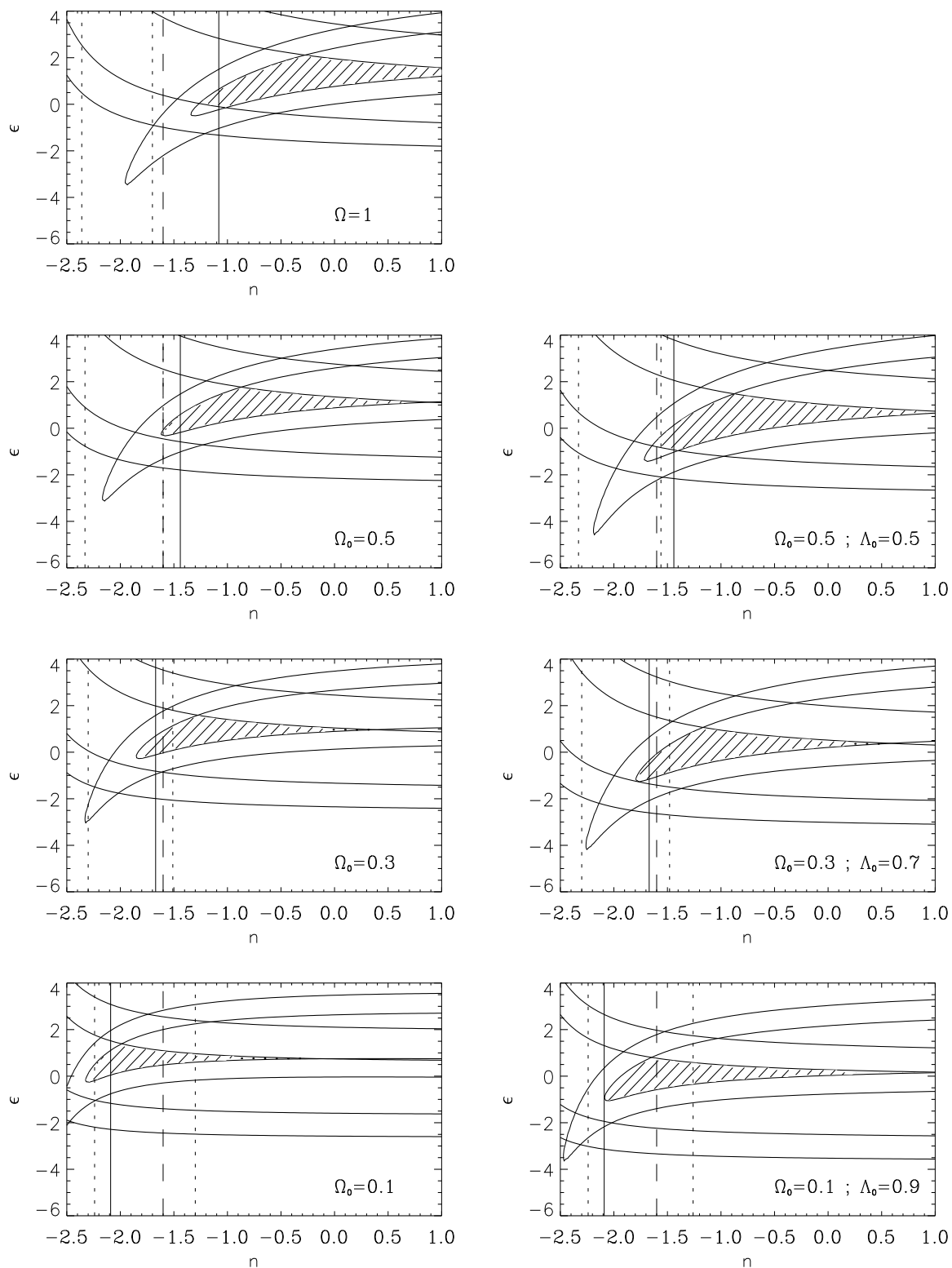


**Figure 7.** Model constraints using the XLF data from the RDCS survey, given by Rosati et al. (1998).

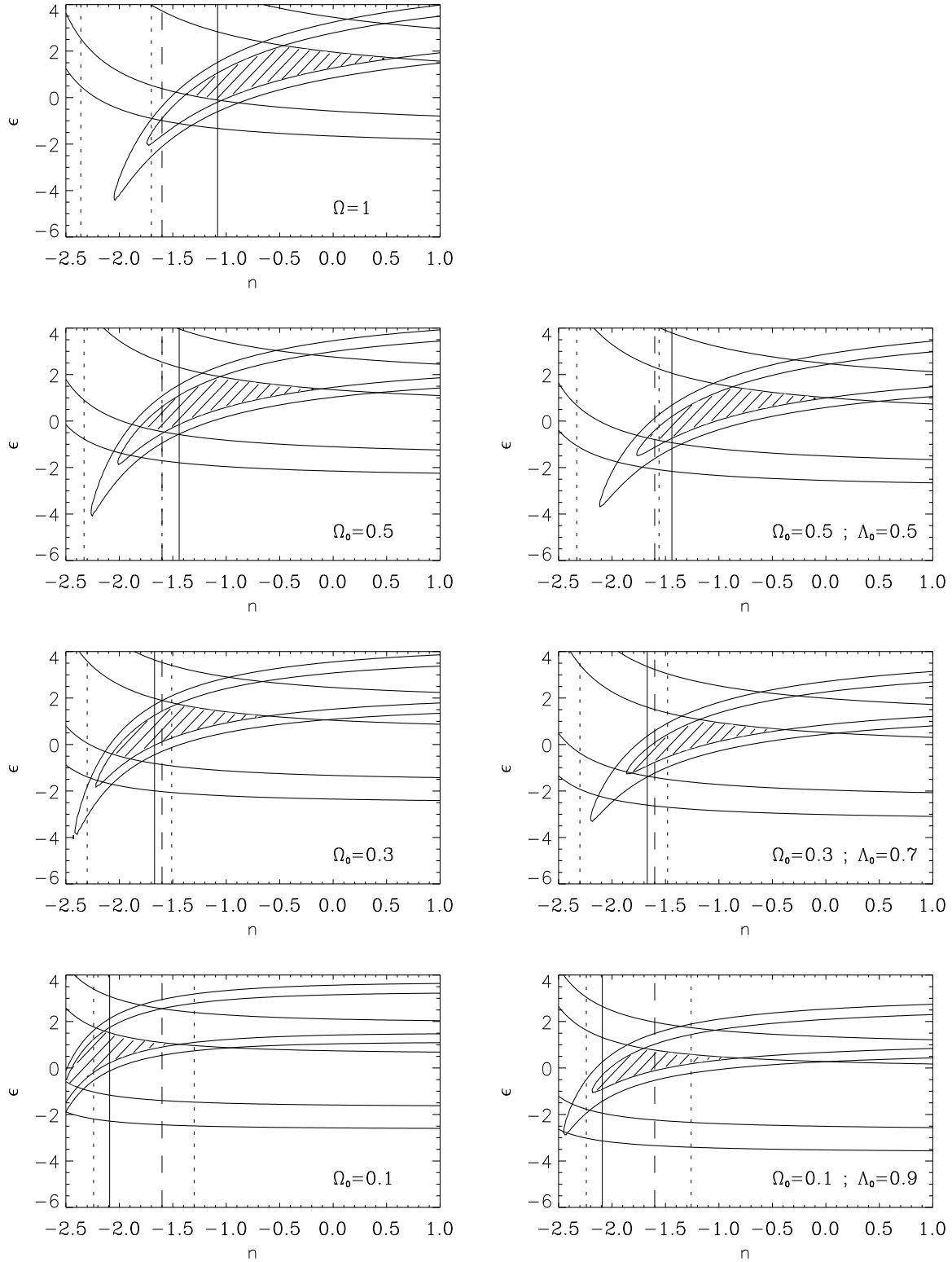


**Figure 8.** Model constraints using the XLF data from the *EMSS* survey, given by Henry et al. (1992).

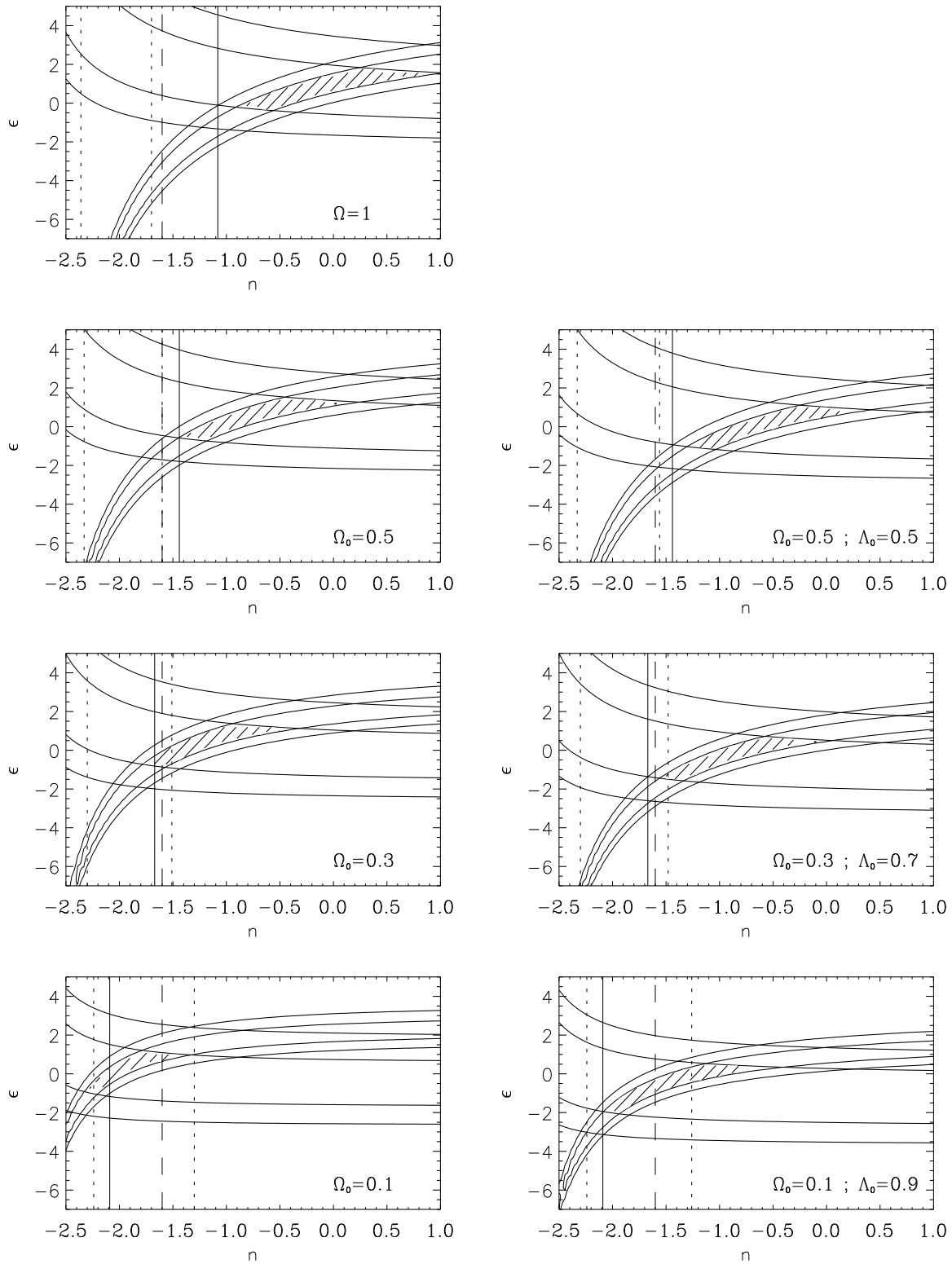


**Figure 9.** Model constraints using the XLF data from the *EMSS* distant cluster sample, given by Luppino & Gioia (1995).

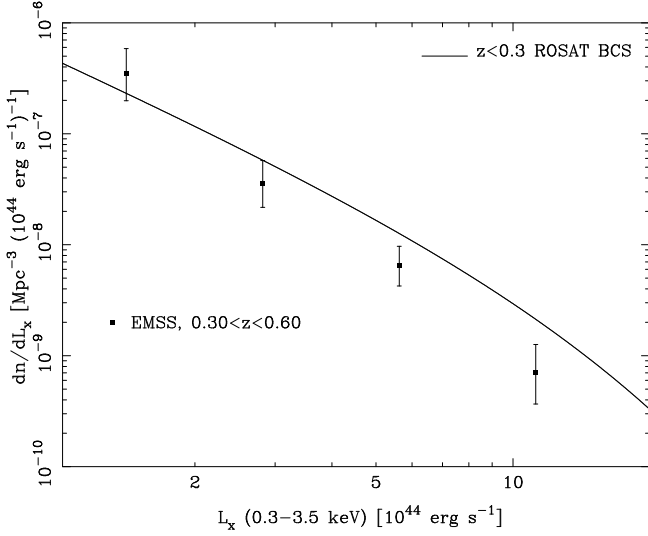


**Figure 3.** The *EMSS* cluster X-ray luminosity function in the 0.3–3.5 keV band, calculated from the work of Henry et al. 1992; again the solid line is the *ROSAT* BCS XLF. For the purposes of this plot,  $q_0 = 0.5$  ( $\Omega = 1$ ).

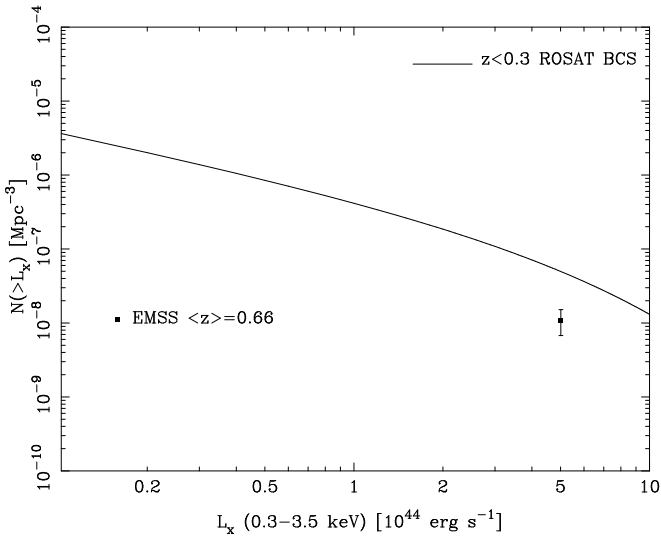


**Figure 4.** The cumulative XLF point from the *EMSS* distant cluster sample ( $N(> 5 \times 10^{44} \text{ erg s}^{-1}) = 1.1 \pm 0.43 \times 10^{-8} \text{ Mpc}^{-3}$ ; Luppino & Gioia 1995), illustrated for the 0.3–3.5 keV band. The solid line is the cumulative version of the *ROSAT* BCS XLF. For the purposes of this plot,  $q_0 = 0.5$  ( $\Omega = 1$ ).

proximate approach. Since little evolution is observed, binning the data in redshift is not likely to result in significant bias. Furthermore, although the selection function is not itself provided, we are provided with predictions for the numbers of clusters expected in a non-evolving model. This information is also given as an estimate of the high-redshift luminosity function. We therefore proceed by adjusting our model parameter so as to predict the correct space density of clusters relative to the non-evolving model. We apply this fitting procedure at the observed median redshift within a wide redshift bin, and use the flux limit of the survey to determine the median luminosity of these clusters. This conversion takes into account the different cosmology assumed

in each model. Although this procedure is non-optimal, we compare only the relative numbers of clusters, thus accurate knowledge of this luminosity limit is not important so long as it is small relative to the curvature of the luminosity function. A second step calculates the number density of clusters at this luminosity relative to the no-evolution and cosmology specific hypothesis used by the survey’s authors. The predicted space density increases because the luminosity limit of the survey is brighter in open cosmologies, but the predicted surface density of clusters on the sky is compensated by the increase in the volume element. The overall correction depends on the slope of the luminosity function at the survey limit, but for the observed values amounts to less than ten percent; much less than the statistical uncertainties in currently available samples.

The constraints placed on the model parameters ( $n, \epsilon$ ) from evolution of the various high-redshift XLF’s (relative to the BCS XLF) for a given cosmology were generated as follows. Firstly, we converted the high-redshift XLF data points to agree with the assumed cosmology. Luminosities are sensitive to cosmology via the area of sky in the flux conversion and number densities in the volume element when calculating the space density, all at the appropriate fixed redshifts. We then assumed that the number of clusters in the  $i^{\text{th}}$  bin ( $N_{clus,i}$ ) were sampled from a Poisson distribution, with the expected number being a function of the true values ( $n^T, \epsilon^T$ ). We calculated the C-statistic for the range of model ( $n, \epsilon$ ) such that  $-2.5 \leq n \leq 1.0$  and  $-6 \leq \epsilon \leq 4$ , where  $C$  is defined as

$$C = -2 \sum_{i=1}^N \ln P_i(N_{clus,i}; E_i(n, \epsilon)), \quad (3.3)$$

$N$  is the number of bins in the high-redshift XLF and  $P_i$  is the probability of observing  $N_{clus,i}$  given  $E_i$ , the expected number of clusters calculated from the model, assuming Poisson statistics. Confidence regions were then calculated by differencing  $C$  with the minimum value (i.e. the most probable set,  $(n_0, \epsilon_0)$ ),  $\Delta C = C - C_{\min}(n_0, \epsilon_0)$ . If  $(n, \epsilon)$  were statistically uncorrelated parameters,  $\Delta C$  would be distributed as  $\chi^2$  with two degrees of freedom (Cash 1979), but we cannot assume here that they are independent. To circumvent this problem, we generated a large number of monte-carlo realisations of each XLF dataset, for all the cosmologies studied. Assuming that the best-fit parameters,  $(n_0, \epsilon_0)$  are the true values (although this method should not depend on this particular choice of parameters), we run the model with a randomly generated dataset and calculated  $\Delta C$  at  $(n_0, \epsilon_0)$ . After a large number of iterations, we then built up a likelihood distribution that should approximate the true likelihood distribution. The confidence levels were then calculated from the values of  $\Delta C$  that incorporated 68% and 95% of the total.

### 3.3 Results

The results we obtained when combining the XLF and  $L_x - T$  normalisation constraints on the model parameters are shown in Figures 5 (SHARC), 6 (WARPS), 7 (RDCS), 8 (*EMSS* 1) and 9 (*EMSS* 2), for a range of feasible values of  $\Omega_0$ , with or without the cosmological constant. Solid contours running from top-left to bottom-right enclose the 68%

and 95% confidence regions for the  $L_x - T$  results and the contours running from top-right to bottom-left enclose the same limits for the measured XLF evolution. Shaded regions are a guide to the eye, highlighting the intersection of the XLF and  $L_x - T$  68% regions.

We note that results from all the datasets analysed show certain common features. Firstly, it is clear that the angles of intersection for the two contour sets are much wider for  $\Omega = 1$ , approaching zero as  $\Omega_0 \rightarrow 0$ . This is due to the fact that the allowed range of  $n$  is increased as the density of the Universe becomes lower. Specifically the lower limit is pushed in the negative direction, since the lowering growth rate can be compensated by a more negative  $n$  to give the same amount of structural evolution. The range of allowed  $\epsilon$  only mildly varies with the value of  $\Omega_0$ , becoming lower as the density decreases, implying that no net entropy evolution is increasingly likely for lower density Universes, with positive values becoming less likely. Individually however, the solutions due to the XLF data show an increase in the limits of  $\epsilon$  as the value of  $\Omega_0$  drops. This is calibrated singularly by the amount of luminosity evolution required to agree with the density evolution (only controlled by  $n$  for a fixed cosmology). The limits from evolution of the  $L_x - T$  normalisation dominate the resultant range of acceptable  $\epsilon$ , showing a more sensitive reaction to cosmology over the XLF limits. This is due to the way in which the measured data points change with cosmology. For the XLF, as  $\Omega_0$  becomes lower, the points move in a very similar direction to the slope of the XLF; both changes in the number density and luminosity conspire to produce a relative shift in the points over the local BCS line that is less sensitive to cosmology than the relative shift in the  $L_x - T$  relation. For the latter, only the luminosity changes, causing positive evolution (in temperature) to be more and more likely as  $\Omega_0$  decreases. Hence, for a fixed value of  $n$ , the acceptable limits on  $\epsilon$  become more negative to decrease the luminosity (at fixed temperature), again the only quantity that depends on  $\epsilon$ .

In comparison to the non-zero  $\Lambda_0$  models, the flat  $\Omega_0 < 1$  models show a slower rate of shift in the acceptable region of parameter space than the corresponding open models. Furthermore, these models have contours that can vary considerably in shape compared to their open counterparts (i.e. same  $\Omega_0$ ), particularly affecting the range of  $n$ . The effects are simply due to the density contribution from the cosmological constant, which causes an increase in the growth rate of structure. This is apparent in the figures, since the results for some flat models look remarkably similar to open models with higher values of  $\Omega_0$  (and hence increased growth rates).

At this stage we would also like to highlight what appears as a discrepancy between the  $\Omega = 1$  constraints in this paper and paper I. It is clear that our 68% regions tend to exclude values of  $n$  that aren't excluded in paper I (e.g.  $n \sim -1.5$ ). This is simply a manifestation of the different XLF constraints - paper I assumed no evolution as the upper limit and a lower limit derived from the RIXOS Survey (Mason et al. 1998), which appears to be incomplete for sources with significant X-ray extent. It is this latter constraint that allows more negative values of  $n$  in paper I than the work presented here.

Due to the considerable number of XLF datasets analysed in this paper, we go to focus on each figure in turn.

### 3.3.1 The SHARC Sample (Figure 5)

The XLF contours essentially circulate the no evolution relation (see Paper I), due to the fact that the XLF points lie very close to the BCS line. The range of allowed  $n$  for given confidence levels is always above some lower limit, which for the 68% case, is  $\sim -1.1$  for  $\Omega = 1$  to  $\sim -2.3$  for  $\Omega_0 = 0.1$ . More negative values would produce too much negative evolution for the given cosmology. Values of  $\epsilon$  tend to centre on a value of zero (no net entropy evolution), although lower values of  $\Omega_0$  allow a larger range negative values.

### 3.3.2 The WARPS Sample (Figure 6)

This sample provides a slightly weaker constraint on the parameters due to the fact that there are, at present, only three bins implemented from this sample. Again, the XLF contours circulate the no evolution contour, with these particular points showing the least amount of evolution in all the samples. Hence the allowed values of  $n$  and  $\epsilon$  are slightly more conservative, although the difference is not exactly significant.

### 3.3.3 The RDCS Sample (Figure 7)

This figure has XLF contours that are shifted to more positive values of  $\epsilon$  than in the previous two. This is due to the fact that the second brightest point on the RDCS XLF is lower than the other two (which comfortably lie on the BCS line), which essentially pulls the bright end of the XLF in the negative direction.

### 3.3.4 The EMSS 1 Sample (Figure 8)

This figure shows the results from the EMSS XLF, illustrating what looks like a considerable amount of negative evolution in abundance. However, lower values of  $\Omega_0$  (predicting less evolution in number density) can still easily fit the data by modifying the luminosity evolution, controlled both by the cosmology and the entropy parameter. The range in luminosities are similar to that of the ROSAT samples (taking the different energy bands into account), although the highest  $L_x$  bin is sufficiently bright to reach  $L_x^*$ , tentatively suggesting an evolving bright end.

### 3.3.5 The EMSS 2 Sample (Figure 9)

The one cumulative (highest-redshift,  $z_c=0.66$ ) XLF point here, again probing brighter luminosities than ROSAT surveys, also indicates what appears to be a deficit of clusters over the local, BCS value. Since there are 6 clusters used to calculate this point, the Poisson errors are comparatively small causing the constrained range of parameter space to form a tight relation between  $n$  and  $\epsilon$ . Furthermore, the XLF at brighter luminosities is more sensitive to changes in luminosity. Hence, it becomes increasingly difficult to compensate the observed change in abundance with luminosity (particularly the core entropy) evolution alone. The lower limit on  $n$  is  $\sim -0.9$  for  $\Omega = 1$  (68%), with the range  $\epsilon$  being almost exclusively positive.

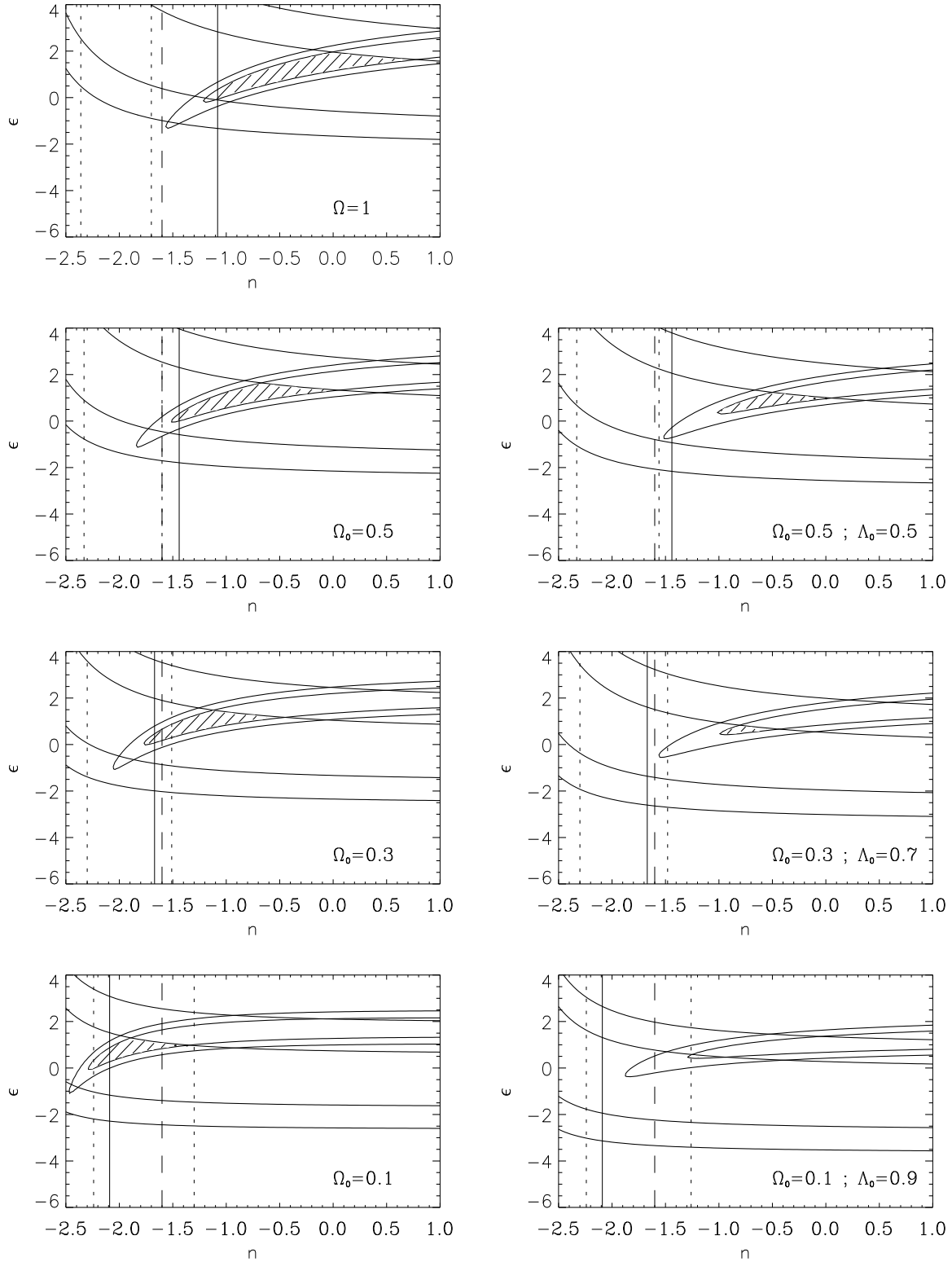


**Figure 10.** Model constraints using all the *ROSAT* XLF data plus the *EMSS* 1 data, shown in the previous figures. The contours from the XLF evolution are chosen to have  $\Delta C$  values to equal  $\Delta\chi^2$  with two degrees of freedom, illustrating regions of 68.3% and 95.4% confidence.

Hence, it is evident that the currently available X-ray data is not sufficient to empirically select a preferred value of  $\Omega_0$ , with or without  $\Lambda_0$ . To high significance, all of the data allows us to find acceptable regions of parameter space for the given background cosmology. The measured *lack* of evolution in the *ROSAT* XLF's provide weak constraints, due to the XLF being fairly insensitive to evolution at the faint end. The *EMSS* samples, particularly the *EMSS 2* cumulative point, start to provide tighter constraints, since these results have started to probe the brighter, more sensitive end. We therefore argue that future surveys such as those using *XMM* data, would be best targetted at the brighter end of the XLF for the range of redshifts that are interesting in rich cluster evolution. We discuss implications of measuring the amount of evolution at the bright end in section 4.3.

To try and obtain a tighter constraint on  $(n, \epsilon)$  for the given cosmologies, we have taken the likelihood distributions from all the *ROSAT* datasets, plus the *EMSS 1* dataset (i.e. all the differential XLF data), and multiplied them to produce a *best-fit*  $\Delta C$  distribution. We have chosen to omit the *EMSS 2* point because the limits set by this data are systematically offset from the other surveys. Our treatment assumes that all points are statistically independent from one another. This may not be wholly justified, since the different *ROSAT* datasets are not completely independent, and may share common fields, since they are all drawn from the same X-ray data archive. Also, any systematic errors in the data analysis will be accumulated and it is not known whether these will dominate over the random Poisson errors, implying that this plot should be interpreted with caution. Figure 10 illustrates the results, with 68.3% and 95.4% confidence regions chosen to have appropriate  $\Delta\chi^2$  values for two degrees of freedom, to give some indication of limits on the likelihood distributions; the same  $L_x - T$  constraints are applied as before. Acceptable regions of parameter space can still be found for the given cosmologies, consistent within current 95% limits on both the XLF and  $L_x - T$  relation, although negative evolution of the bright end pushes up the contours to higher values of  $\epsilon$ , which becomes a problem for more open Universes, and the lack of evolution at the faint end pushes the range of  $n$  to more positive ranges for higher  $\Omega_0$  and/or flat models with non-zero  $\Lambda_0$ . For the present, we note that since the range of acceptable  $n$  is more sensitive to the value of  $\Omega_0$ , independent measurements of the slope of the power spectrum on rich cluster scales may provide further constraints on the value of  $\Omega_0$ . We now go on to investigate this.

### 3.4 Breaking the $n$ - $\Omega_0$ degeneracy

It is evident that the model is unable to determine any preferred value of  $\Omega_0$  from the XLF and  $L_x - T$  normalisation constraints alone - a feasible range of  $n$  can always be found for the particular scenario. Furthermore, the constrained range of  $\epsilon$  does not vary much for  $\Omega_0 \leq 1$ . Hence, to break the *degeneracy* between  $n$  and  $\Omega_0$ , an independent determination of  $n$  is required. There are two ways in which this can be achieved - a theoretical determination of the primordial power spectrum that gives the (cosmology-dependent) slope on rich cluster scales or a direct measurement from imaging surveys. We look at both methods here, which we detail below. For the theoretical case, we need to obtain the local

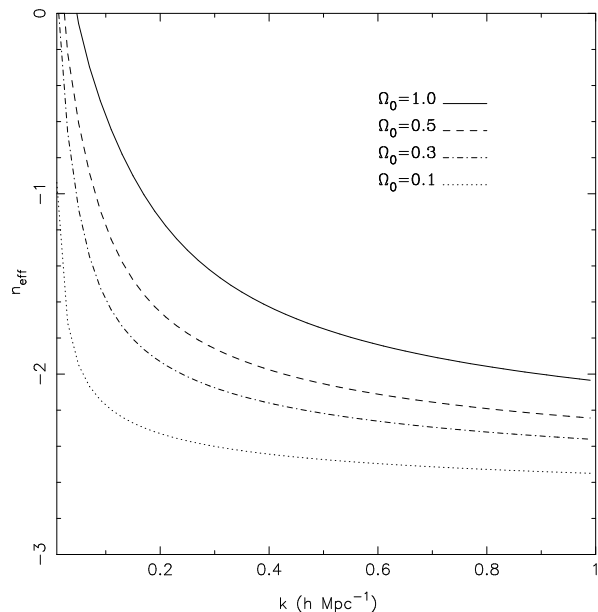


**Figure 11.** The effective slope of the CDM power spectrum as a function of scale for the four values of the density parameter studied in this paper.

slope of the power spectrum on rich cluster scales,  $n_{\text{eff}}$  such that

$$n_{\text{eff}} = \left. \frac{d \ln P}{d \ln k} \right|_{k_{\text{eff}}} \quad (3.4)$$

where  $P(k) \propto k^{-3} \Delta^2(k)$ . Although there has been feverous debate recently, the currently most popular cosmogony is that dominated by cold dark matter (CDM), with  $n \rightarrow 1$  for small  $k$ , turning over to  $n \sim -3$  on small scales. We use the transfer function given by Bardeen et al. (1986). The turnover scale is determined by the shape parameter,  $\Gamma$ , which is where the cosmological information enters, specifically

$$\Gamma = \Omega_0 h \exp \left[ -\frac{\Omega_b}{\Omega_0} (\Omega_0 + \sqrt{2h}) \right] \quad (3.5)$$

(Sugiyama 1995). We take the value  $\Omega_b = 0.013 h^{-2}$  from nucleosynthesis constraints (Copi, Schramm & Turner 1995). No contribution enters from the cosmological constant, due to the fact that it contributed negligibly to the energy density at the last scattering epoch. To estimate  $k_{\text{eff}}$ , we assume that the virial mass of a typical rich cluster in the local Universe (e.g. the Coma cluster) is  $M \sim 5 \times 10^{14} h^{-1} M_\odot$ . If the cluster formed by the top-hat collapse of a spherically overdense region, the comoving radius required to contain this mass (assuming present background density) would be  $R \sim 8 h^{-1} \text{Mpc}$  (Eke, Cole & Frenk 1996). This is only true for a critical density Universe but can easily be modified for lower densities, since  $R \propto \Omega_0^{-\frac{1}{3}}$ . The value of  $R$  can then be converted to an effective scale on the linear power spectrum by using the following formula (Peacock & Dodds 1994)

$$k_R = \left[ \frac{[\frac{1}{2}(n+1)]!}{2} \right]^{\frac{1}{n+3}} \frac{\sqrt{5}}{R} \quad (3.6)$$

which should iteratively converge on the set  $[n_{\text{eff}}, k_{\text{eff}}]$ , with the use of equation 3.4. Figure 11 shows the variation of  $k_{\text{eff}}$  with  $n_{\text{eff}}$  for the four values of  $\Omega_0$  studied. Clearly for a fixed scale, the value of  $n$  becomes more negative as  $\Omega_0$  drops. This is due to the fact that the value of  $\Gamma$  is becoming lower, leading to a shift in the position of the turnover in the CDM spectrum to larger scales. The calculated values of  $n$  are represented as solid lines in the model constraints plots discussed in section 3.3. Although the scale of rich clusters changes with  $\Omega_0$  causing  $n$  to become less negative as  $\Omega_0$  drops, the sensitivity of  $n$  to this is quite small, hence the former effect dominates. Unfortunately, the constrained values of  $n$  moves in the same direction, allowing us to make no more conclusions to what the value of  $\Omega_0$  is. However, if the results of co-adding the results from all of the XLF data are to be believed, only significantly low values of  $\Omega_0$  ( $+\Lambda_0 = 0$ ) are consistent with the CDM calculation.

Another method is to constrain  $n$  directly by measuring the power spectrum on rich cluster scales from wide-area sky surveys. One example (Tadros, Efstathiou & Dalton 1997) comes from the APM cluster sample, which has a median redshift  $\langle z \rangle = 0.09$ , measuring a slope,  $n_{\text{APM}} \sim -1.6$ . We currently assume that the underlying power spectrum has negligible curvature on the range of scales we are studying. Ideally, we would separate the population into redshift bins and scale each respective population relative to the preceding one, using the slope of the spectrum at that epoch. Imminent surveys such as the Sloan Digital Sky Survey and the 2dF Galaxy Redshift Survey should provide the necessary data to constrain the slope at higher redshifts. Furthermore, we also assume that the bias is linear and therefore scale-invariant - with the justification that any deviations from linearity would be expected to occur on smaller scales, as result of local environmental effects.

To do this, we have taken the likelihood distributions of each dataset, fixing the value of  $n$  to the APM value. We then looked for the range of  $\Omega_0$  (with and without  $\Lambda_0$ ) that is consistent in the  $\epsilon$  direction with both the XLF and  $L_x - T$  evolution limits, by finding their point of intersection. This was done for both 68% and 95% confidence limits. We found that since the range of  $n$  becomes larger (specifically in the negative direction) as  $\Omega_0$  drops, it is impossible to place a lower limit on  $\Omega_0$ ; the model fits the data more and more adequately as the Universe becomes progressively less dense. However, it is still possible to place an upper limit on the value of  $\Omega_0$ .

The results on this limit are displayed in Table 3, displaying the values that are consistent with both the 68% and 95% confidence limits of the XLF and  $L_x - T$  relations. The ranges in brackets were determined by varying the value of  $n$  by  $\pm 0.3$ , the uncertainty quoted by the authors. Firstly, we note that at the 68% level, we can rule out a critical density Universe for all datasets, with the exception of the WARPS and *EMSS* 1 data, if  $n$  was at it's minimum,  $-1.3$ . The values are even stronger when including the cosmological constant, with the exception of the RDCS case. The results are all mainly affected by the growth rate:  $\Lambda_0$  models are equivalent in some sense to having a larger  $\Omega_0$  in the open case. Although the RDCS is peculiar in the sense that it has a data point lying significantly lower than the others and the BCS line, hence geometrical effects have affected the model solutions. For the 95% limits, we cannot place an

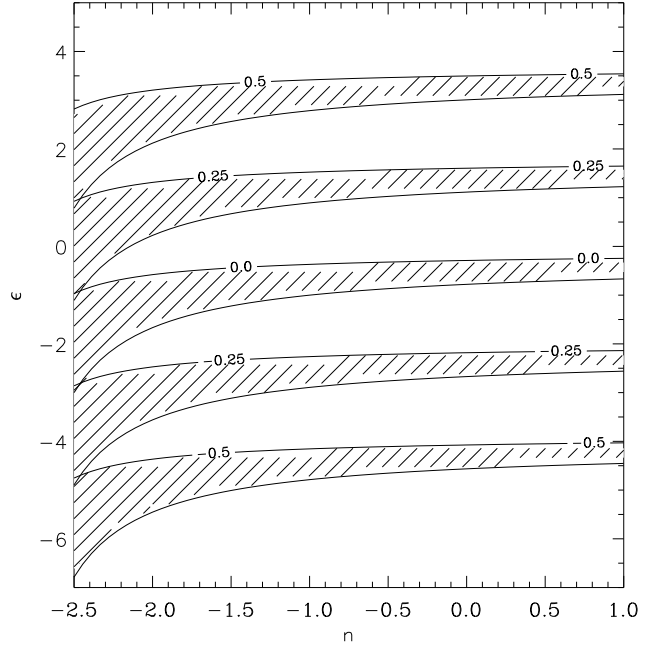


**Figure 12.** The region of parameter space covered by evolution of the cluster core radius for various models. The shaded regions depict the range of cosmologies, from  $\Omega = 1$  (with the greatest amount of structure evolution) to  $\Omega = 0.1, \Lambda_0 = 0.0$  (with the least amount of structure evolution). Each particular area illustrates the different amount of evolution in the redshift range  $z = [0.0, 0.5]$ , with the labels indicating the value  $\Delta \log r_c$ .

upper limit on the value of  $\Omega_0$  below 1.0 for  $n = -1.6$  with the exception of the *EMSS* 2 point (which shows the most amount of evolution) - the same applies for the  $\Lambda_0$  models.

It is apparent, therefore, that from the inclusion of the slope measurement, the value of  $\Omega_0$  has to be lower than 0.75, consistent with all of the data, at least at the 68% level in the individual datasets. There's a considerable degree of scatter in the absolute upper limit of  $\Omega_0$ , which is not only due to the positions of the points but the total number of clusters in each sample being small. We have also included limits placed on  $\Omega_0$  from the combined datasets (with the exception of the *EMSS* 2 point), as displayed in Figure 10. The effect is much more startling in this case, to the extent that the value of  $\Omega_0 > 0.3$  is too high in the non-zero  $\Lambda_0$  cases to be consistent with the power spectrum measurement (at the 95% level) - otherwise a low  $\Omega_0$  open Universe is required. This strategy is open to systematic uncertainties, as we discussed earlier, but it is clear that future measurements with well controlled cluster selection and X-ray flux measurements will be able to provide a tight constraint.

### 3.5 Evolution of Cluster Core Sizes

Another potential constraint on the model parameters can come from measuring the evolution of the cluster core size, which we predict to scale as

$$r_c \propto \delta_+^a (1+z)^b (1+z_f)^c \left( \frac{\Delta_{\text{vir}}}{\Omega} \right)^d \quad (3.7)$$



Survey	$\Omega_{0,u}$ (68%, $\Lambda_0 = 0$ )	$\Omega_{0,u}$ (68%, $\Omega_0 + \Lambda_0 = 1$ )	$\Omega_{0,u}$ (95%, $\Lambda_0 = 0$ )	$\Omega_{0,u}$ (95%, $\Omega_0 + \Lambda_0 = 1$ )
SHARC	0.45 [0.25, 0.7]	0.15 [0.1, 0.4]	1.0 [0.6, > 1.0]	1.0 [0.5, > 1.0]
WARPS	0.75 [0.45, > 1.0]	0.7 [0.35, > 1.0]	> 1.0 [0.75, > 1.0]	> 1.0 [0.7, > 1.0]
RDCS	0.5 [0.25, 0.95]	0.6 [0.25, > 1.0]	> 1.0 [0.65, > 1.0]	> 1.0 [0.65, > 1.0]
<i>EMSS</i> 1	0.7 [0.45, > 1.0]	0.65 [0.25, > 1.0]	> 1.0 [0.7, > 1.0]	> 1.0 [0.55, > 1.0]
<i>EMSS</i> 2	0.45 [0.25, 0.65]	0.35 [0.2, 0.6]	0.7 [0.45, > 1.0]	0.65 [0.35, > 1.0]
COMBINED DATA	0.4 [0.25, 0.8]	0.05 [0.03, 0.1]	0.9 [0.45, > 1.0]	0.3 [0.1, > 1.0]

**Table 3.** Upper limits on the value of  $\Omega_0$  (with and without  $\Lambda_0$ ), using the constraint that  $n = -1.6$ , from the APM survey (Tadros, Efstathiou & Dalton, 1997). The last row is for the combination of the first four datasets, as discussed earlier. Results are for 68% and 95% confidence limits, consistent with both the XLF and  $L_x - T$  constraints. Ranges in square brackets are for quoted uncertainties in  $n$  ( $\pm 0.3$ )

$$\begin{aligned}
 a &= \frac{2}{n+3} \left(1 - \frac{1}{\beta}\right) \\
 b &= \frac{\epsilon}{2\beta} \\
 c &= \frac{1}{2\beta} - 1 \\
 d &= \frac{1}{3} \left(\frac{1}{2\beta} - 1\right)
 \end{aligned}$$

in comoving co-ordinates. Even though the core radius depends on both  $n$  and  $\epsilon$ , we argue that its evolution is determined much more sensitively by the changes in the central entropy of the gas rather than the amount of structural evolution. Figure 12 illustrates this by plotting various amounts of core radius evolution out to a redshift  $z = 0.5$ . We show here that the background cosmology and spectral index have no real determination on the evolution of  $r_c$ , but observations should quite easily place a constraint on the value of  $\epsilon$  - the two extremes in the figure represent scaling in the core by a factor of  $\sim 0.3$  and 3 respectively. Core sizes that shrink with redshift demand negative values of  $\epsilon$  (i.e. the core entropy of clusters decreases with redshift) where core sizes that grow with redshift demand values of  $\epsilon$  that are at least, weakly negative. Using this approach is useful in the sense that we can directly measure the rate of entropy evolution in the core and test its consistency with the other methods for determining the values of the free parameters. Analysis involving looking at changes in the cluster core size has now started to appear in the literature. Results are currently suggesting no significant evolution in the proper core size, at least out to  $z \sim 0.5$  (Vikhlinin et al. 1998), implying that the cores become larger with redshift in the comoving frame. Hence, this hints at values of  $\epsilon$  that are approximately zero, consistent with the range as determined by the data analysed previously. We hope to pursue this in more detail, in the near future.

## 4 DISCUSSION

We have shown that current measurements of the evolution of the XLF and  $L_x - T$  correlation do not by themselves constrain the cosmological density parameter  $\Omega_0$ . Although lower values of  $\Omega_0$  imply a slower rate of cluster growth, this can be compensated by adopting a flatter power spectrum and adjusting the entropy evolution parameter  $\epsilon$ . Additional

constraints need to be applied to restrict the allowed values of  $\Omega_0$ , such as an independent constraint on the the slope of the power spectrum. For values of the power spectrum consistent with the large scale power of the APM survey ( $n = -1.6$ , Tadros, Efstathiou & Dalton 1997), the data point to  $\Omega_0 < 0.75$  ( $\Omega_0 < 0.7$ , for  $\Omega_0 + \Lambda_0 = 1$ ) at the 68% confidence level, although they do not rule out  $\Omega = 1$  at the 95% level.

We have left it until this stage to address several points that may have left the reader wondering. Firstly, our results are based on several important assumptions made when modelling the X-ray evolution of clusters, so we discuss our choices and their robustness. Secondly, particularly due to the recent publication of *ROSAT* and *ASCA* data, the subject of cosmology from an X-ray cluster perspective has been a hot topic of late. We therefore dedicate a section to comparatively discuss our results with other groups. Finally, we address what we think is an important strategy for observations, particularly with the imminent launch of the *XMM* satellite, and pin-point the areas that we think will maximise future success in this field.

### 4.1 Model Assumptions

Although general and based on physically required scaling relations, there are several key approximations in the model used to arrive at this conclusion. One example is the  $\beta$  profile: the results presented in §3 assume that the X-ray emission profiles are well fit by using the  $\beta$  - model, where the density of the intracluster gas tends to a constant value at small  $r$  (the core) and the singular isothermal result at large  $r$ , for a value of  $2/3$ . Individual measurements of  $\beta$  do not necessarily give this value, although we assume that the average value over the population at a given epoch is well represented by  $\langle \beta \rangle = 2/3$ . However, it is important to investigate the tolerance of the model when varying the value of  $\beta$ . Figure 13 illustrates the effect on the constrained range of  $n$  and  $\epsilon$  that variations of  $\beta$  induces. Using the SHARC data as an example, we have taken three values of  $\beta$  : 0.6,  $2/3$  and 0.7, with the first and last defining what we think are the expected limits of any fluctuation. Two cosmological models have been chosen :  $\Omega = 1$  and  $\Omega_0 = 0.1$ , which represent the most and least amount of structural evolution respectively. The most striking result is that changing  $\beta$  can significantly change the range of  $\epsilon$  values but has relatively little effect

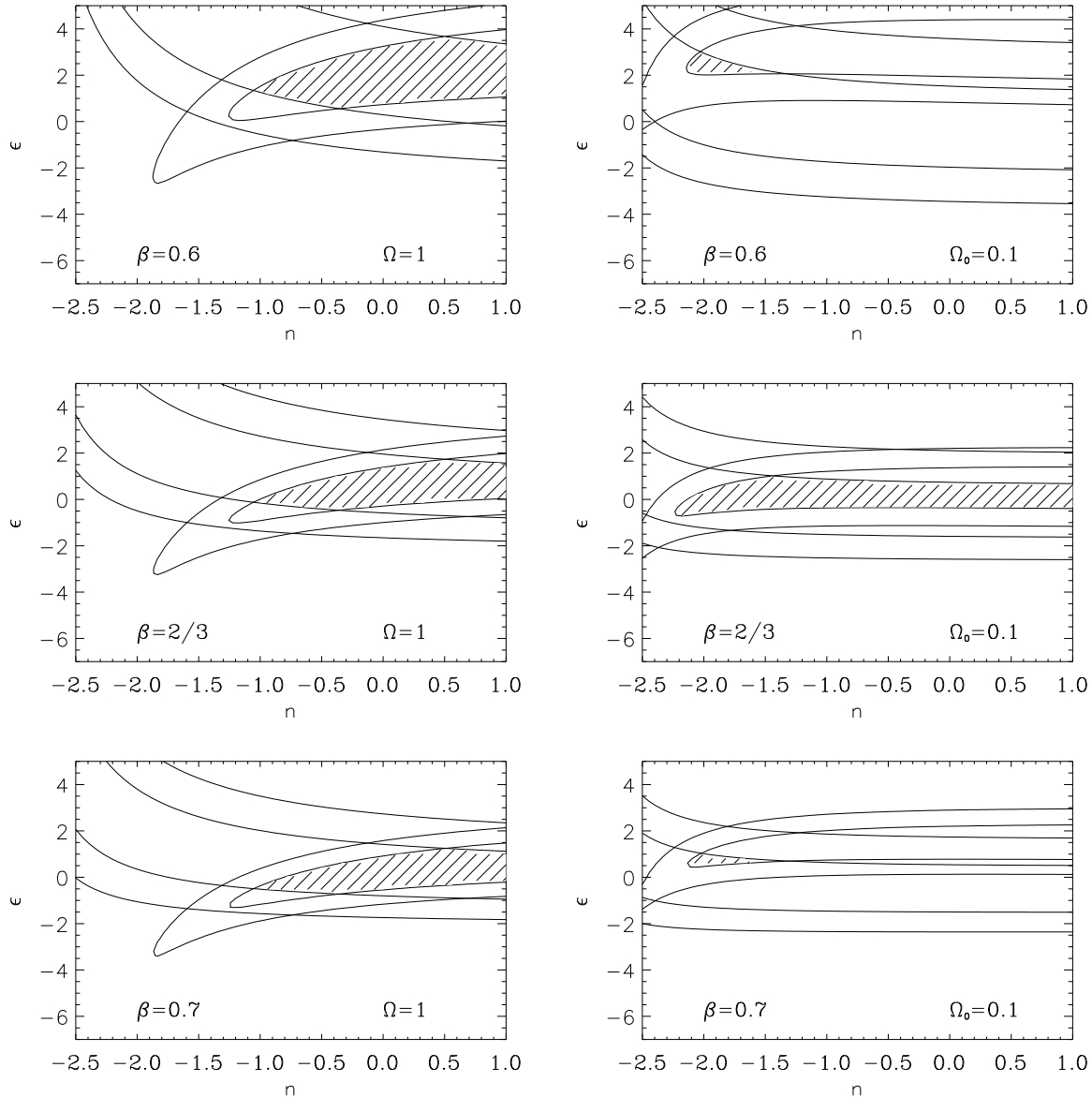


**Figure 13.** An example of the effect of varying  $\beta$  using the SHARC XLF data. The left column is for  $\Omega = 1$  (the most mass evolution) and the right column  $\Omega_0 = 0.1$  (the least mass evolution). The middle row is the canonical value of  $2/3$  used for analysis in this paper, with the top and bottom rows for the expected limits on  $\beta$  (0.6 and 0.7 respectively). The effect on  $n$  is insignificant, although raising  $\beta$  lowers the range of  $\epsilon$ .

on the values of  $n$ . This, coupled with the work on the core radius discussed in the last section, reinforces the idea that both  $n$  and  $\epsilon$  contribute separately to the evolution of clusters: the entropy evolution is sensitive to the way in which the gas is distributed, with  $\beta$  and  $r_c$  defining the shape of the density profile, while the mass evolution is tied in with the background density. Hence, the dependence of  $\Omega_0$  on  $\beta$  is weak, although certain models may be ruled out on the basis that the range of  $\epsilon$  may be out of range. This is evident in the figure, where the combination ( $\beta = 0.6, \Omega_0 = 0.1$ ) pushes allowed values of  $\epsilon$  into the limit set by the maximum cooling calculation ( $\epsilon = 2.0$ ) given in Paper I.

With the Launch of the *AXAF* satellite, it will become possible to study the emission profiles of distant clusters in

more detail. These studies may show that the cluster profile evolves with redshift. For example, simulations of cluster evolution with pre-heated gas by Mohr & Evrard (1997) suggests that the entropy injected reduces the overall slope of the gas density profile rather than just that of the profile of the very centre. This effect can be parameterised by a much slower role over near the core radius - but the scaling of the solution remains the same, since the X-ray emission still scales as  $\rho_c^2 r_c^3 T^\alpha$ . Thus, as Figure 13 shows, the  $\beta$  profile and the  $\epsilon$  parameter are interconnected - while observations of the emission profiles of high redshift clusters would cause us to revise our physical interpretation of a particular  $\epsilon$  value, and re-examine the balance of heating and cooling within

the cluster, it would not invalidate the phenomenological description provided by the model.

We may apply the same argument to take into account the non-isothermal temperature of structure of clusters (Markevitch et al. 1998). The model only requires that the temperature structure is normalised by the virial temperature of the dark matter halo. The temperature structure may affect the rate at which the cluster core evolves for a given entropy change, but this should again be taken into account when the  $\epsilon$  parameter is interpreted.

As we have developed it, this model for X-ray evolution applies to clusters of galaxies that are in dynamical equilibrium. Clusters that are seen during major mergers may have X-ray luminosities and average temperatures that are far from their hydrostatic values. Nevertheless, the description we have developed applies to the cluster population as a whole, and the properties of individual clusters may differ wildly from the smooth trends in the population as a whole. In this sense, the effects of mergers are incorporated through the entropy evolution described by the model, and the disruption of hydrostatic equilibrium is mimicked by an increase in core entropy. The effect of departures from hydrostatic equilibrium on the luminosity of the clusters is thus already accounted for in the model. The cluster temperatures are also susceptible to these departures, however, since they are weighted by the luminosity. Ideally, we should use cluster temperatures measured from the outer regions of clusters where the gas temperature better reflects the virial temperature of the gravitational potential. These are not available for distant clusters at present, but our results will still be valid so long as the evolution of the luminosity weighted temperature reflects the evolution of the cluster potential. This is a problem common to all methods based on the X-ray temperatures of clusters.

The slope of the luminosity-temperature correlation does not explicitly enter our determination for the evolution of clusters. All that is required in our model is the evolution of the normalisation. We have implicitly assumed that the slope remains fixed at its present-day value. This assertion, which corresponds to the assumption that the entropy evolution parameter ( $\epsilon$ ) is independent of cluster temperature, is unavoidable with the limited temperature data that is available for high redshift clusters. Consequently, it is important that the evolution of the normalisation is determined by using consistent slopes for high and low redshift data, and preferably using high redshift cluster representative of the clusters used to determine the luminosity function evolution. At present, temperature measurements are available only for the brightest clusters at high redshift. This situation will hopefully improve with the launch of the *XMM* satellite (Lumb et al. 1996); its large collecting area is ideally matched to the determination of temperatures for the lower luminosity, distant clusters. The slope of nearby ( $z < 0.05$ ) clusters has been most recently determined by Markevitch (1998), using *ROSAT* luminosities and *ASCA* temperatures, measuring a value,  $\lambda \sim 2.65$ . However, we make use of the older sample based on *EMSS* MPC data (David et al. 1993) for two reasons. Firstly, constraints on the evolution of the  $L_x - T$  relation are provided by MS97, which uses this (local) sample to contrast with their higher redshift ( $< z > \sim 0.3$ ) *ASCA* data. Also, the slope supplied by Markevitch has been calculated for clusters with cooling

flows removed, in order to directly compare with models that exclude non-radiative components in the plasma evolution. Since our model is based on evolution of the central entropy, we cannot exclude the cooling flow clusters, which probably contribute to most, if not all of the negative entropy evolution in cluster populations. We argue that the dominant cause for the intrinsic scatter in the relation is due to each cluster having its own particular core entropy, coming from their individual formation histories.

## 4.2 Comparison with Other Methods

The considerations we discussed above related to the distribution of gas within the dark matter potential. In a low density universe, it is necessary to explicitly account for the distinction between the background density of the Universe when the cluster is formed, and its value when the cluster is observed. We have related these two epochs by assuming that the mass of the cluster grows by a factor of two (Kitayama & Suto, 1996). However, for  $\Omega_0 > 0.1$ , this factor produces only a small change in the halo evolution.

A number of other papers have recently appeared in the literature dealing with the constraints on  $\Omega_0$  from the X-ray evolution of clusters. One of the most popular methods at present is using the evolution of the cluster abundances (e.g. Eke et al. 1998, Henry 1997, Viana & Liddle 1998, Mathiesen & Evrard 1998, Oukbir & Blanchard 1997, Reichart et al. 1998). To extract the value of  $\Omega_0$ , an estimator for the cluster virial mass is required. This can be achieved by calculating the cluster temperature function at any given epoch and converting this to mass using the Press-Schechter formalism with the assumption that the cluster haloes form via spherical infall. The result from this method is still slightly unclear - at present the majority find values of  $\Omega_0$  typically in the region 0.3 - 0.5 with or without  $\Lambda$ , although some authors find higher values including  $\Omega = 1$  (e.g. Sadat et al. 1998, Blanchard & Bartlett 1998, Reichart et al. 1998). An extensive discussion on the existence of this clash in results can be found in Eke et al. (1998). In particular, they highlight the discrepancy in the abundance of low-redshift clusters, particularly the high temperature end, where the measured value is uncertain. Those favouring high  $\Omega_0$  assume a higher abundance of clusters in this region than those favouring low values of  $\Omega_0$ .

Our work differs from these treatments in that it does not assume a detailed model for the abundance of clusters or for their temperature or X-ray luminosity distribution. Instead, we have emphasised the scaling relations that must relate the properties of clusters at one epoch with those at another. By introducing an additional parameter that describes the evolution of the core gas entropy, our approach allows us to intercompare clusters at different epochs with minimal further assumptions. Comparing our results with those authors illuminates those constraints which are general and those that are model-specific. As an example, Reichart et al. (1998) also look at luminosity function evolution by adopting the Press-Schechter approach for the evolution of the mass function, but use the  $L_x - T$  relation to calibrate their mass to X-ray luminosity relation. In addition, their model differs from ours in that it involves the slope of the  $L_x - T$  relation explicitly, resulting in a purely empirical calibration of the luminosity mass conversion. By contrast,

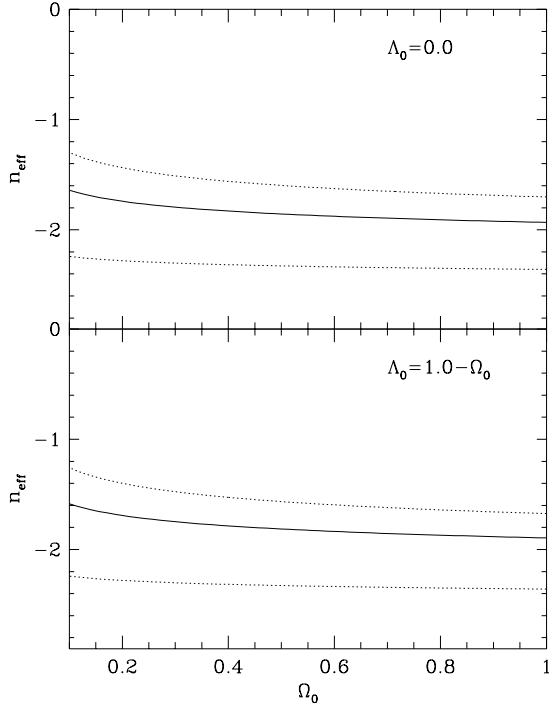


**Figure 14.** The relation between  $n_{eff}$  and  $\Omega_0$  for the measured values of  $\Gamma$  given by Eke et al. (1998), for the range of cosmological scenarios studied in this paper, at  $z = 0$ . The solid lines are the best-fit values and the dotted lines are the quoted limits.

our approach uses the weak self-similarity principle (plus the entropy evolution) to scale the properties of clusters between epochs. As discussed extensively in Paper I, this is completely separate from the relations between clusters of different mass at the same epoch. Trying to equate the two requires that we adopt a Strong Self-Similarity principle; something for which there is little physical justification. Reichart et al. adopt the same parameterization as Evrard & Henry (1991), notably  $L_x \propto T^p(1+z)^s$ ; assuming  $\beta = 2/3$ , we find for our model that  $p = 13/6$  and  $s = (13 - 3\epsilon)/4$ . However, as we have emphasised, the way in which we constrain our parameters (particularly  $\epsilon$  in this context) is fundamentally different, and we should not expect to obtain identical results.

We choose to concentrate our comparison with the work of Eke et al. (1998), using luminosity function data derived from the *EMSS* survey (Henry et al. 1992). These authors derive a value of  $\Omega_0$  from the evolution of the cluster temperature function using cluster emission-weighted temperatures from the the *ASCA* satellite (Henry 1997). They take into account the X-ray flux limited nature of the cluster sample by assuming a constant  $L_x - T$  relation with fixed, non-evolving scatter, using this to correct for the incompleteness in the temperature function. This method has the benefit of inferring the mass distribution directly, but requires samples with complete temperature information and well-defined completeness. Their work gives a strong constraint on  $\Omega_0$ :  $\Omega_0 = 0.44 \pm 0.2$  for  $\Lambda_0 = 0$  and  $\Omega_0 = 0.38 \pm 0.2$  with a non-zero cosmological constant. This constraint is significantly stronger than that which we derive, and furthermore,

the authors were able to constrain the effective power spectrum internally. The constraint on the power spectrum (assuming the CDM paradigm) arises because they directly link the form of the temperature function to the mass function through the Press-Schechter model. They arrive at a value of  $\Gamma$  of  $0.08 \pm 0.07$  ( $\Gamma = 0.09 \pm 0.08$  for  $\Omega_0 + \Lambda_0 = 1$ ), which translates to values of  $n$  that are illustrated in Figure 14, using the same CDM transfer function discussed in section 3.4. On its own, this restriction only limits our determination of  $\Omega_0$  to values below 0.75 (0.7 for non-zero  $\Lambda$ ). This is to be expected, since our work is inherently a deconvolution process. However, they have also incorporated the assumption that the  $L_x - T$  correlation is non evolving, to correct for incompleteness. If we were also to make this assumption we would obtain comparable results for the upper limit:  $\Omega_0 < 0.55$ . At higher  $\Omega_0$ , the non-evolving  $L_x - T$  relation requires too large an  $\epsilon$  value to be consistent with XLF evolution; however we cannot provide a lower limit as they do. This is initially surprising, but seems to be due to the systematic differences between the datasets. We find that, for a low  $\Omega_0$  cosmology, the available data are consistent with no evolution of both the XLF and  $L - T$  relation. For very low values of  $\Omega_0$ , the model also predicts little evolution (with appropriate choice of  $\epsilon$ ) and is thus fully consistent. For high values of  $\Omega_0$ , the XLF and  $L_x - T$  data requires values of  $\epsilon$  to fit the luminosity evolution required, that are inconsistent for the range of appropriate  $n$ . By contrast, Eke et al.’s temperature function data (corrected for cosmology) show a decline in temperature function amplitude suggesting that a very low value of  $\Omega_0$  is unacceptable due to the deficit of clusters at this epoch. Such dependence on the particular data set is worrying, but emphasises the importance of using independent data-sets to establish consistent conclusions and reduce systematic biases. However, we are inherently limited in our comparison by the difference in models used, although it is satisfying to find that our method finds similar results, at least in determining the upper limit. Overall, we conclude that the constraints placed by Eke et al., result in a large part from the tight constraint that they place on the shape of the temperature function. This requires additional physical input that our approach does not attempt to model, connecting the shape of the power spectrum to the shape of the luminosity or temperature function. The particular properties of the *EMSS* cluster sample also play a role. We are not able to place as tight a constraint on the value of  $\Omega_0$ , primarily due to the extra uncertainty that is introduced by the deconvolution of luminosity and entropy evolution.

### 4.3 Future Directions

Since the results presented in this paper were based on scaling the *ROSAT* BCS XLF (assumed to be representative of the present day distribution) to fit the higher redshift surveys, we have assumed that the two populations are well separated; unfortunately we do not have the full datasets, which would allow us to optimise the bin selection to maximise the probability of detecting cosmological evolution. This is not immediately obvious, since the *ROSAT* BCS sample has clusters out to  $z \sim 0.3$ , where the other samples start around this value. The saving grace is that the higher-redshift surveys have detected lower luminosity clusters ( $L_x \sim L_x^*$ ) due to the small solid angles of the surveys,

where the BCS clusters in this regime are at much lower redshifts. However, this range of luminosities places a much weaker constraint on the model than if data were available at the brighter end (to the right of the *knee* of the XLF) ; improved coverage will result in a better internal constraint since the effects of evolving cluster number density and cluster luminosity will be more easily separated.

A more sound statistical description of the XLF at the bright end will thus determine whether a trade-off from high and low  $\Omega_0$  is required (negative evolution), or that high values of  $\Omega_0$  can be ruled out if no evolution was detected. As discussed earlier (Figure 10), the modestly evolving bright end, measured at present, combined with a non-evolving faint end, cannot separate out the different cosmological models, although only the low  $\Omega_0$  open models appear to be consistent with the estimated slope of the power spectrum on rich cluster scales (ruling out flat,  $\Omega_0 > 0.3$  models at 95%). As a pointer for the future, we propose that what is required, in order to be able to separate the models based on the X-ray data alone, is a more statistically sound description of the high-redshift XLF from  $L_x^*$  and above. As an example, adding the *EMSS* 2 point, for which there is significant negative evolution around  $L_x^*$ , demands that flat models with  $\Omega_0 > 0.1$  can be ruled out with complete confidence from the XLF and power spectrum constraint alone. Alternatively, if we assume the case that no evolution was a fair description at both the bright and faint ends, specifically if ten clusters were detected at a redshift  $z = 0.5$  with  $L_x(0.5 - 2.0 \text{ keV}) = 10^{45} \text{ ergs}^{-1}$  and a solid angle that resulted in an abundance that agreed with the BCS cumulative XLF ( $N(> L_x) \sim 0.25 \times 10^{-8} \text{ Mpc}^{-3}$ ), and the SHARC data points are a good representation of the faint end, values of  $\Omega_0 > 0.5$  are ruled out at the 95% level, using the  $n_{\text{APM}}$  constraint. The *XMM* satellite is particularly suited to this task, with its large collecting area and high spatial resolution that will allow one to easily make the distinction between clusters and AGN. What is required, however, is a wide area survey covering at least 500 square degrees, rather than a survey that is particularly deep. In the near term, progress will be made through the *ROSAT* North Ecliptic Pole survey - a wide angle survey composed of superposed *ROSAT* All-Sky Survey strips (Gioia et al. 1998).

## 5 CONCLUSIONS

In this paper, we have taken the entropy-driven model of cluster evolution, detailed in Bower (1997) for an  $\Omega = 1$  Universe, and modified it to account for evolution in different cosmological scenarios - specifically open models and flat, non-zero  $\Lambda$  models. This allows us to separate contributions made by the hierarchical growth of structure (controlled by the slope of the power spectrum,  $n$ ) and changes in the core entropy of the intracluster gas (via the entropy evolution parameter,  $\epsilon$ ).

We then placed constraints on  $n$  and  $\epsilon$  for seven reasonable cosmological models, using the current wave of X-ray data for the two observables: the X-ray Luminosity Function and the Luminosity-Temperature relation. For the luminosity-temperature relation, we have taken the compiled low and high redshift samples from David et al. (1993) and Mushotzky & Scharf (1997) respectively and determined

the best-fit slope and scatter. We subsequently placed 68% and 95% confidence limits on the evolution of the temperature normalisation, which is slope-dependent. For the XLF, we have used the recently available *ROSAT* samples, specifically the SHARC (Burke et al. 1997), WARPS (Jones et al. 1998) and RDCS (Rosati et al. 1998) high-redshift, non-parametric determinations, as well as the older *EMSS* samples (Henry et al. 1992, Luppino & Gioia 1995). The amount of evolution in these measurements was quantified by comparing with the local *ROSAT* BCS XLF (Ebeling et al. 1997). The main results are that we find acceptable regions of parameter space for all the data (combining the XLF and  $L_x - T$  results), in every cosmological model considered, to a high degree of confidence. The range of X-ray luminosities are currently not-sufficient to determine any acceptable range of  $\Omega_0$  (with or without the cosmological constant), using this method. Specifically, as the density parameter decreases, more negative values of  $n$  are allowed to compensate for the weakening growth rate of clusters. Values of constrained  $\epsilon$  are appropriate to modify the luminosity evolution to compensate for the measured change in abundance, moving weakly from positive values to zero (no evolution) for low-density Universes.

To say something more about the most likely values of the cosmological parameters, we calculated the slope of the power spectrum based on the CDM paradigm, by taking the typical mass of a rich cluster and calculating the corresponding fluctuation scales that give rise to such objects. We find that the CDM calculation does not help in separating the different cosmological models - the scale is always consistent with the data. We also applied the measured value from the APM survey,  $n = -1.6$  and concluded that all data were individually consistent with this value for  $\Omega_0 < 0.75$  ( $< 0.7$  for  $\Omega_0 + \Lambda_0 = 1$ ), using the 68% confidence regions of the individual datasets. Combining the *ROSAT* datasets, plus the *EMSS* dataset of Henry et al., we find that  $\Omega_0 < 0.9$  for open models, at the 95% level. Flat models with  $\Omega_0 > 0.3$  are ruled out for the same degree of confidence. We cannot determine a lower limit to the value of  $\Omega_0$ , since our model fits the data much more comfortably for lower density Universes.

The evolution of cluster core-radii were also considered, where we showed that it depended much more sensitively to the entropy evolution of clusters than the structural evolution (determined by  $n$  and  $\Omega_0$ ). Recent results point to no net entropy evolution, consistent with the other measurements.

Finally, we discussed the robustness of assumptions we have made in the model, particularly the effect of varying the mass distribution of the gas (controlled by the value of  $\beta$ ). Again, this has a much stronger effect on the constrained range of  $\epsilon$  than the rate of structural evolution, and hence only weakly affects the determination of  $\Omega_0$ . We then compared our results to that of other groups, particularly with Eke et al. (1998). Using the *EMSS* XLF of Henry et al. (1992) and no evolution in the  $L_x - T$  relation, in order to try and be consistent with their data, we find that our upper limit is consistent ( $\Omega_0 < 0.55$ ) although we cannot place a lower limit on  $\Omega_0$ . However, we find that the amount of evolution calculated for the normalisation of the  $L_x - T$  relation allows higher values of  $\Omega_0$ . This is again due to the

extra freedom allowed by the  $\epsilon$  parameter in the luminosity evolution of the samples.

In order to provide better limits on the value of  $\Omega_0$ , it will be essential to obtain an accurate high-redshift measurement of the bright end of the XLF, ideally from a wide angle survey out to modest redshifts. This is something we hope that the forthcoming *XMM* mission can provide.

## ACKNOWLEDGEMENTS

The paper would not have been completed without the generous help of Doug Burke, Piero Rosati and Laurence Jones with their XLF data and Vince Eke, Shaun Cole and Carlos Frenk for useful discussions. This project was carried out using the computing facilities supplied by the Starlink Project. STK and RGB acknowledges the support of a PPARC post-graduate studentship and the PPARC rolling grant for “Extragalactic Astronomy and Cosmology at Durham” respectively.

## REFERENCES

- Bardeen J.M., Bond J.R., Kaiser N., Szalay A.S., 1986, *ApJ*, 304, 15
- Blanchard A., Bartlett J.G., 1998, *A&A*, submitted (*astro-ph/9712078*)
- Bower R.G., Smail I., 1997, *MNRAS*, 290, 292
- Bower R.G., 1997, *MNRAS*, 288, 355
- Bower R.G. et al. 1996, *MNRAS*, 281, 59
- Burke D.J., Collins C.A., Sharples R.M., Romer A.K., Holden B.P., Nichol R.C., 1997, *ApJ*, 488, L83
- Cash W., 1979, *ApJ*, 228, 939
- Castander F.J. et al., 1995, *Nature*, 377, 39
- Collins C.A., Burke D.J., Romer A.K., Sharples R.M., Nichol R.C., 1997, *ApJ*, 479, L117
- Copi C.J., Schramm D.N., Turner M.S., 1995, *Science*, 267, 192
- David L.P., Slyz A., Jones C., Forman W., Vrtilik S.D., 1993, *ApJ*, 412, 479
- De Grandi S., Molendi S., Bohringer H., Chincarini G., Voges W., 1997, *ApJ*, 486, 738
- Dekel A., Burstein D., White S.D.M., 1997, *Critical Dialogues in Cosmology* (Princeton 250th Anniversary) ed. N. Turok (World Scientific), p175 (*astro-ph/9611108*)
- Ebeling H., Edge A.C., Fabian A.C., Allen S.W., Crawford C.S., Bohringer H., 1997, *ApJ*, L479, 101
- Eke V.R., Cole S.M., Frenk C.S., Henry J.P., 1998, *MNRAS*, submitted (*astro-ph/9802350*)
- Eke V.R., Navarro J.F., Frenk C.S., 1998, *ApJ*, in press (*astro-ph/9708070*)
- Eke V.R., Cole S.M., Frenk C.S., 1996, *MNRAS*, 282, 263
- Evrard A.E., 1989, *ApJ*, 341, L71
- Evrard A.E., Henry J.P., 1991, *ApJ*, 383, 95
- Gioia I.M., Luppino G.A., 1994, *ApJS*94, 583
- Gioia I.M. et al., 1998, in preparation
- Hasinger G., Burg R., Giacconi R., Schmidt M., Trumper J., Zamorani G., 1998, *A&A*, 329, 482
- Henry, J.P., 1998, in preparation
- Henry, J.P., 1997, *ApJ*, 489, L1
- Henry J.P., Gioia I.M., Maccacaro T., Morris S.L., Stocke J.T., Wolter A., 1992, *ApJ*, 386, 408
- Jones C., Forman W., 1984, *ApJ*, 276, 38
- Jones L.R., Scharf C., Perlman E., Ebeling H., Horner D., Wegner G., Malkan M., McHardy I., 1998, *AN*, 319, 87
- Kaiser N., 1991, *ApJ*, 383, 104
- Kaiser N., 1986, *MNRAS*, 222, 323
- Kitayama T., Suto Y., 1997, *ApJ*, 490, 557
- Kitayama T., Suto Y., 1996, *ApJ*, 469, 480
- Lacey C., Cole S., 1993, *MNRAS*, 262, 627
- Lacey C., Cole S., 1994, *MNRAS*, 271, 676
- Lahav O., Rees M.J., Lilje P.B., Primack J.R., 1991, *MNRAS*, 251, L128
- Luppino G.A., Gioia I.M., 1995, *ApJ*, 445, L77
- Lumb, D., Eggel, K., Laine, R., Peacock, A., 1996, *SPIE*, 2808, 326
- Markevitch M., 1998, *ApJ*, submitted (*astro-ph/9802059*)
- Markevitch M., Forman W.R., Sarazin C.L., Vikhlinin A., 1998, *ApJ*, submitted (*astro-ph/9711289*)
- Mason K.O. et al., 1998, *MNRAS*, submitted
- Mathiesen B., Evrard A.E., 1998, *MNRAS*, submitted (*astro-ph/9703176*)
- Mohr J.J., Evrard A.E., 1997, *ApJ*, 491, 38
- Mushotzky R.F., Scharf C.A., 1997, *ApJ*, L485, 65
- McHardy I.M. et al. 1998, *AN*, 319, 51
- Navarro J.F., Frenk C.S., White S.D.M., 1997, *ApJ*, 490, 493
- Oukbir J., Blanchard A., 1997, *A&A*, 317, 10
- Peacock J.A., Dodds S.J., 1994, *MNRAS*, 267, 1020
- Peebles P.J.E., *The Large-Scale Structure of the Universe*, 1980, PUP, Princeton, NJ
- Press W.H., Schechter P., 1974, *ApJ*, 187, 425
- Reichart D.E., Nichol R.C., Castander F.J., Burke D.J., Romer A.K., Holden B.P., Collins C.A., Ulmer M.P., 1998, *ApJ*, submitted (*astro-ph/9802153*)
- Rosati P., Ceca R.D., Norman C., Giacconi R., 1998, *ApJ*, 492, L21
- Sadat R., Blanchard A., Oukbir J., 1998, *A&A*, 329, 21
- Scharf C.A., Jones L.R., Ebeling H., Perlman E., Malkan M., Wegner G., 1997, *ApJ*, 477, 79
- Smail I., Ellis R.S., Dressler A., Couch W.J., Oemler A., Butcher H., Sharples R.M., 1997, *ApJ*, 479, 70
- Sugiyama N., 1995, *ApJS*, 100, 281
- Tadros H., Efstathiou G., Dalton G., 1997, *MNRAS*, submitted (*astro-ph/9708259*)
- Tsuru T., Koyama K., Hughes J.P., Arimoto N., Kii T., Hattori M., 1996, *The 11th international colloquium on UV and X-ray spectroscopy of Astrophysical and Laboratory Plasmas*
- Viana P.T.P., Liddle A.R., (*astro-ph/9803244*)
- Vikhlinin A., McNamara B.R., Forman W., Jones C., Quintana H., Hornstrup A., 1998, *ApJ*, in press (*astro-ph/9803101*)
- White S.D.M., Efstathiou G., Frenk C.S., 1993, *MNRAS*, 262, 1023